1 **Formation of condensable organic vapors from anthropogenic and**

2 **biogenic VOCs is strongly perturbed by NOx in eastern China**

3

4 Yuliang Liu[1,2], Wei Nie[1,2]*, Yuanyuan Li[1,2], Dafeng Ge[1,2], Chong Liu[1,2], Zhengning

5 Xu[1,2,5], Liangduo Chen[1,2], Tianyi Wang[1,2,10], Lei Wang[1,2], Peng Sun[1,2], Ximeng Qi[1,2],

6 Jiaping Wang[1,2], Zheng Xu[1,2], Jian Yuan[1,2], Chao Yan[3], Yanjun Zhang[3,9], Dandan

7 Huang[4], Zhe Wang[6], Neil M. Donahue[7], Douglas Worsnop[8], Xuguang Chi[1,2], Mikael

8 Ehn[3], and Aijun Ding[1,2]

9

10 [1] Joint International Research Laboratory of Atmospheric and Earth System Sciences, School of

11 Atmospheric Sciences, Nanjing University, Nanjing, Jiangsu Province, China

12 [2] Collaborative Innovation Center of Climate Change, Jiangsu Province, China

13 [3] Institute for Atmospheric and Earth System Research/Physics, Faculty of Science, University of

14 Helsinki, Helsinki, Finland

15 [4] State Environmental Protection Key Laboratory of Formation and Prevention of Urban Air

16 Pollution Complex, Shanghai Academy of Environmental Sciences, Shanghai, China

17 [5] College of Environmental & Resource Sciences, Zhejiang University, Zhejiang, China

18 [6] Department of Civil and Environmental Engineering, the Hong Kong Polytechnic University,

19 Hong Kong SAR

20 [7] Center for Atmospheric Particle Studies, Carnegie Mellon University, Pittsburgh, PA, USA

21 [8] Center for Aerosol and Cloud Chemistry, Aerodyne Research Inc., Billerica, MA, USA

22 [9] Univ. Lyon, Université Claude Bernard Lyon 1, CNRS, IRCELYON, 69626, Villeurbanne, France

23 [10] Meteorological Service Center of Hubei Province, Wuhan, 430074

24

Abstract

25

26

27 Oxygenated organic molecules (OOMs) are the crucial intermediates linking volatile

28 organic compounds (VOCs) to secondary organic aerosol (SOA) in the atmosphere, but

29 understandings on the characteristics of OOMs and their formations from VOCs are

30 very limited. Ambient observations of OOMs using recently developed mass

31 spectrometry techniques are still limited, especially in polluted urban atmosphere where

32 VOCs and oxidants are extremely variable and complex. Here, we investigate OOMs,

33 measured by a nitrate-ion-based chemical ionization mass spectrometer at Nanjing in

34 eastern China, through performing positive matrix factorization on binned mass spectra

35 (binPMF). The binPMF analysis reveals three factors about anthropogenic VOCs

36 (AVOCs) daytime chemistry, three isoprene-related factors, three factors about biogenic

37 VOCs (BVOCs) nighttime chemistry, and three factors about nitrated phenols. All

38 factors are influenced by NOx in different ways and to different extents. Over 1000 non-

39 nitro molecules have been identified and then reconstructed from the selected solution

40 of binPMF, and about 72% of the total signals are contributed by nitrogen-containing
41 OOMs, mostly regarded as organic nitrates formed through peroxy radicals terminated
42 by nitric oxide or nitrate-radical-initiated oxidations. Moreover, multi-nitrates account
43 for about 24% of the total signals, indicating the significant presence of multiple
44 generations, especially for isoprene (e.g., $C_5H_{10}O_8N_2$ and $C_5H_9O_{10}N_3$). Additionally, the
45 distribution of OOMs concentration on carbon number confirm their precursors driven
46 by AVOCs mixed with enhanced BVOCs during summer. Our results highlight the
47 decisive role of NO_x on OOMs formation in densely populated areas, and encourage
48 more studies on the dramatic interactions between anthropogenic and biogenic
49 emissions.
50
51 **1 Introduction**
52
53 Secondary organic aerosol (SOA), as an important and complex component of
54 submicron particles (Zhang et al., 2007;Jimenez et al., 2009;Huang et al., 2014), is fully
55 involved in affecting climate (Intergovernmental Panel on Climate, 2014) and causing
56 health risks (Nel, 2005;Lim et al., 2012). Volatile organic compounds (VOCs) are
57 ubiquitous in the atmosphere and are recognized as main precursors of SOA (Hallquist
58 et al., 2009;Ziemann and Atkinson, 2012). However, the missing intermediate processes
59 from VOCs to SOA are yet to be elucidated (Hallquist et al., 2009;Ehn et al., 2014).
60
61 Benefitting from the state-of-the-art measurement technics (Bertram et al.,
62 2011;Jokinen et al., 2012;Lee et al., 2014), many previously unreported oxygenated
63 organic molecules (OOMs), as intermediates from VOCs to SOA (Ziemann and
64 Atkinson, 2012), have been discovered. Among OOMs, highly oxygenated organic
65 molecules (HOMs), first observed in the gas phase at a boreal forest site (Ehn et al.,
66 2010;Ehn et al., 2012) and have been reviewed by Bianchi et al. (2019), are so
67 functionalized and low volatile that they can participate at the beginning of new particle
68 formation (NPF) by stabilizing sulfuric acid (Kulmala et al., 2013;Riccobono et al.,
69 2014) or through clustering alone (Kirkby et al., 2016;Bianchi et al., 2016), and
70 condense on existing particles to be responsible for a large fraction of SOA (Ehn et al.,
71 2014). In addition to conventional VOCs-to-OOMs mechanisms summarized in the
72 Master Chemical Mechanism (MCM) (http://mcm.york.ac.uk/, last access: 09 February
73 2021), recent studies have proposed new pathways, such as autoxidation (Crounse et
74 al., 2013;Jokinen et al., 2014) and multigenerational oxidation (Rollins et al.,
75 2012;Wang et al., 2020b), to form condensable vapors by adding oxygen atoms
76 efficiently. The productions of OOMs, especially HOMs, from precursors such as
77 monoterpenes (Ehn et al., 2014;Jokinen et al., 2015;Kirkby et al., 2016;Berndt et al.,
78 2016), sesquiterpenes (Richters et al., 2016), isoprene (Jokinen et al., 2015;Zhao et al.,
79 2020) , aromatics (Wang et al., 2017;Molteni et al., 2018;Garmash et al., 2020), and
80 alkanes (Wang et al., 2021) have been investigated in laboratories by using the chemical
81 ionization atmospheric pressure interface time-of-flight mass spectrometer with nitrate
82 reagent ions (nitrate CI-APi-TOF).
83

84   New insights and a general understanding about OOMs have been attained, yet many
85   critical details about OOMs formation and properties need to be addressed. First, the
86   current kinetic descriptions of OOMs obtained from experiments are still limited, such
87   as the lack of individual H-shift rates for autoxidation and of reaction rates of multi-
88   generational products with oxidants. Furthermore, the complexity of the real
89   atmosphere makes it more difficult to apply experimental results to ambient
90   environments. The precursors compete for oxidants and vice versa, and their products
91   will interact mechanistically in mixtures of atmospheric vapors (McFiggans et al.,
92   2019;Heinritzi et al., 2020). However, in the laboratory we usually study simple
93   systems with a single precursor and a single oxidant. Moreover, most experiments are
94   carried out for environments dominated by biogenic VOCs (BVOCs), while
95   anthropogenic emissions receive less attention. In addition to classic anthropogenic
96   VOCs (AVOCs), large amounts of primary emissions of oxygenated VOCs are also
97   present in urban areas (Karl et al., 2018). The effect of NOx on OOMs is another key
98   issue. NO_x can terminate peroxy radicals (RO_2), outcompeting autoxidation
99   propagation reactions and other bimolecular reactions ($RO_2 + RO_2$, $RO_2 + HO_2$), and
100   change the products distribution, and consequently, size-dependently modulate the
101   growth rates of organic aerosol particles (Yan et al., 2020). Additionally, NO_x
102   contributes non-linearly to atmospheric oxidants, which also influence the productions
103   of OOMs (Pye et al., 2019). It is anticipated that NO_x plays a varied role in the
104   formations of OOMs as well as SOA in different environments.
105
106   Therefore, more extensive OOMs observations are needed to validate the atmospheric
107   implications of experiments, to couple with the global or regional model, and finally to
108   comprehensively understand the fate of OOMs in the atmosphere. Until now, only a
109   few ambient observations of OOMs using nitrate CI-APi-TOF have been reported
110   (Bianchi et al., 2019), and almost all of them focus on rural or forested or remote
111   atmospheres (Yan et al., 2016;Massoli et al., 2018;Zhang et al., 2020;Beck et al., 2021).
112
113   The Yangtze River delta (YRD) is one of the most developed regions in eastern China.
114   Fine particulate matter, with an aerodynamic diameter smaller than 2.5 μm ($PM_{2.5}$), has
115   been significantly reduced in eastern China after the implementation of "Action Plan
116   for Air Pollution Prevention and Control" since 2013 (Ding et al., 2019), while
117   (secondary) organic aerosol are still much more abundant than in clean areas (Zhang et
118   al., 2017;Sun et al., 2020). Here we investigated condensable oxygenated organic
119   vapors observed by nitrate CI-APi-TOF in August-September 2019 at the Station for
120   Observing Regional Processes and the Earth System (SORPES) in the western part of
121   the YRD, an anthropogenic-emissions-dominated environment (Fu et al., 2013;Xu et
122   al., 2017) mixed with enhanced biogenic emissions during summer (Wang et al.,
123   2020a;Xu et al., 2021). A variety of oxidants (Liu et al., 2019;Li et al., 2020;Xia et al.,
124   2020) with numerous precursors (VOCs) suggest very complicated atmospheric
125   oxidation processes and thousands of products (OOMs). Thereby, positive matrix
126   factorization (PMF) (Paatero and Tapper, 1994) was applied to time-resolved mass
127   spectra which had been pre-divided into small bins (binPMF, Zhang et al., 2019), to

128 separate various sources or processes of OOMs. Combined with summarizing the
129 ensemble chemical characteristics of OOMs, some interesting inspirations about the
130 conversion of VOCs to OOMs were obtained.

131

132 **2 Methodology**

133

134 **2.1 Study site**

135

136 The SORPES station (32°07′14″ N, 118°57′10″ E; 62 m a.s.l.) is located at Nanjing in
137 the western part of YRD, one of the most developed regions in eastern China. Due to
138 its unique location, this site can be influenced by air masses from different source
139 regions of anthropogenic emissions, biomass burning, dust and biogenic emissions
140 (Ding et al., 2013;Ding et al., 2016). Detailed descriptions for the station can be found
141 in previous studies (Nie et al., 2015;Xie et al., 2015;Xu et al., 2018;Wang et al.,
142 2018a;Sun et al., 2018;Shen et al., 2018).

143

144 **2.2 Instrumentation**

145

146 The nitrate CI-APi-TOF (Aerodyne Research Inc. and Tofwerk AG), combining a
147 chemical ionization source (CI) and an atmospheric pressure interface time-of-flight
148 mass spectrometer (APi-TOF) equipped with a long-TOF model (LTOF) with mass
149 resolution of 8000-12000 Th/Th, was deployed to detect the ambient sulfuric acid and
150 OOMs. The ambient air was pulled into a laminar flow reactor, where the sample flow
151 (10 L min^{-1}) is surrounded by a purified airflow serving as the sheath flow (25 L min^{-1}
152), through a stainless-steel tube (a 100 cm long, 3/4 in. diameter). Nitrate reagent ions
153 were generated in the sheath flow by exposing air-containing nitric acid to a
154 PhotoIonizer X-Ray (Model L9491, Hamamatsu, Japan). Detailed description of the
155 instrument has been described elsewhere (Junninen et al., 2010;Jokinen et al., 2012).
156 The data were acquired at 1 Hz time resolution and analyzed with a tofTools package
157 (version 6.11) based on MATLAB (MathWorks Inc.). The quantification of OOMs was
158 derived via Eq. (1).

159

160
$$[OOM_i] = \ln\left(1 + \frac{\sum_{n=0}^{1}[OOM_i \cdot (HNO_3)_n \cdot NO_3^- + (OOM_i - H)^-]}{\sum_{n=0}^{2}[(HNO_3)_n \cdot NO_3^-]}\right) \times C \times T_i \tag{1}$$

161 Here $[OOM_i]$ is the concentration (molecules cm^{-3}) of the OOM molecule. On the right
162 side of the equation, the numerator in the parenthesis is the observed total signals (ions/s)
163 of OOM ions charged in different way, the denominator is the sum of all reagent ion
164 signals (ions/s). First, a H$_2$SO$_4$-based calibration factor C (4.2×10^9 molecules cm^{-3}) was
165 inferred from a calibration using H$_2$SO$_4$ (Kuerten et al., 2012) proceeding taking into
166 account the diffusion loss in the sampling line, by assuming that all detected OOMs
167 have the same ionization efficiency as H$_2$SO$_4$ and that the (OOM·NO$_3$-) clusters are
168 very stable without dissociation during their residence time of detection. Second, a mass
169 dependent transmission efficiency T_i of APi-TOF was inferred in a separate experiment
170 by depleting the reagent ions with several perfluorinated acids (Heinritzi et al., 2016).

171
172 VOCs precursors were measured by a proton transfer reaction time-of-flight mass
173 spectrometer (PTR-ToF-MS, Ionicon Analytik, Innsbruck, Austria, TOF 1000 ultra).
174 $PM_{2.5}$ was measured with a combined technique of light scattering photometry and beta
175 radiation attenuation (Thermo Scientific SHARP Monitor Model 5030). The chemical
176 compositions of $PM_{2.5}$ was determined on-line using time-of-flight aerosol chemical
177 speciation monitor (TOF-ACSM, Aerodyne Research Inc.). PMF analysis was further
178 used to separate the organic aerosol (OA) to primary and secondary organic aerosols
179 (POA and SOA). The number concentrations of particles were measured by the
180 scanning mobility particle sizer (SMPS) with nano DMA (4.0 to 63.8 nm) and long
181 DMA (41.4 to 495.8 nm) and the aerodynamic particle sizer (APS) (0.5 to 18.0 μm).
182 NO and NO_2 were measured using a chemiluminescence analyzer equipped with a blue-
183 light converter (TEI, Model 42I-TL); O_3, SO_2, and CO were measured using the
184 ultraviolet photometry, pulsed-UV fluorescence, and IR (infrared) photometry
185 techniques (TEI, Model 49I, 43C, and 48C), respectively. Zero and span calibrations
186 for trace gases were performed weekly during the campaign. Meteorological
187 measurements including relative humidity (RH), wind speed, wind direction, and air
188 temperature were recorded by Automatic Weather Station (CAMPEEL co., AG1000).
189 $J(O^1D)$ was measured by ultra-fast CCD-detector spectrometer, UVB enhanced
190 (Meteorologieconsult Gmbh, Germany).
191
192 **2.3 Hydroxyl radical (OH) estimate**

193 The OH concentration was calculated by applying the Eq. (2), based on the assumption
194 that gaseous sulfuric acid (SA) is mostly produced from the oxidation of SO_2 by OH
195 and primarily loss by condensing onto particles, denoted as condensation sink (CS). It
196 has been proved that $\frac{k_{OH+SO_2}\cdot[SO_2]\cdot[\cdot OH]}{CS}$ is a very reliable proxy for SA during the day
197 (Lu et al., 2019). The ozonolysis of alkenes can form stabilized Criegee intermediates
198 (SCIs) in addition to OH, and SCIs can also oxidize SO_2 to form SA (Mauldin Iii et al.,
199 2012;Guo et al., 2021). A previous study on SA proxy in this site has revealed that the
200 reactions of SO_2 with products from the ozonolysis of alkenes generate a moderate
201 amount of nighttime sulfuric acid, with little effect on daytime sulfuric acid (Yang et
202 al., 2021). Thus, OH may be overestimated during nighttime. In this study, OH was
203 used to calculate the production rates of RO_2 (Fig. 4), the error of OH do not change
204 the relative distribution of RO_2 from different precursors. And OH is mainly used when
205 analyzing daytime data.
206

207
$$[OH] = \frac{SA \cdot CS}{k_{OH+SO_2} \cdot [SO_2]}$$
(2)

208
209 **2.4 binPMF**
210

211   binPMF has been used to analyze the measured HR mass spectrometry data. Briefly,
212   the raw spectra with were divided into narrow bins with a width of 0.006 Th after mass
213   calibration. The data matrix and error matrix were prepared according to the methods
214   described by Zhang et al. (2019) for the PMF model inputs (Section S1 in the
215   supplement). Different from the traditional PMF such as using unit mass resolution
216   (UMR) or HR data as input, binPMF still retains HR information as much as possible,
217   avoids the uncertainty of HR peak fitting influencing the results of PMF, and separate
218   the complex overlapping peaks for fitting. The PMF analysis in this work uses the
219   IGOR based analyzing interface SoFi (solution finder, version 6.8) and ME-2 as
220   described in (Canonaco et al., 2013). After select the PMF solution, we fitted the HR
221   peaks in each factor through toftool.
222

223   **3 Results and Discussions**

224

225   Figure 1 shows temporal variation of OOMs and related parameters at the SORPES
226   station in the northeastern suburb of Nanjing from August 02 to September 06, 2019.
227   During the observation period, 22 of 35 days had maximum hourly temperatures above
228   30 degrees Celsius, and 29 days had maximum hourly $J(O^1D)$ above 2×10^{-5} s^{-1}. High
229   temperature and solar radiation indicate strong photochemistry, producing a large
230   amount of ozone, with concentration often exceeding 80 ppb. Even at night, the
231   concentration of ozone is rarely lower than 10 ppb, resulting from the weak titration of
232   low NO. At the same time, the reaction between ozone and high concentration of NO_2
233   can provide sufficient NO_3 radicals, dominating nocturnal degradation of certain
234   volatile organic compounds (VOCs) (Wayne et al., 1991). The elevated mixing level of
235   total aromatic hydrocarbons is one of the main characteristics of the atmosphere in
236   densely populated areas, in addition to which there should be many alkanes and alkenes
237   which cannot be observed by PTR-ToF-MS (Fu et al., 2013;Xu et al., 2017). In the
238   daytime with strong photochemical reaction ($J(O^1D)> 1\times10^{-5}$ s^{-1}), we instead observed
239   higher concentrations of isoprene than total aromatics ([isoprene]$_{median}$=1.3 ppb,
240   [aromatics]$_{median}$=1.1 ppb). The complex mixtures of anthropogenic and biogenic VOCs
241   can be oxidized through a variety of pathways to produce OOMs, of which some low
242   volatile components will condense into particles, forming organic aerosol. The
243   concentrations of OOMs with mass-to-charge ratio (m/z) below 360 Th are usually
244   higher than 10^6 molecules cm^{-3}, and some can even reach up to 10^7-10^8 molecules cm^{-}
245   ^{3}. Clustered peaks on the spectra of OOMs and their clear daily variations imply a lot
246   of chemical and physical dynamics information (Fig. 1(d), see Fig. S1(a) for normalized
247   spectra), which is the main aspect we want to explore in this work.

248

Atmospheric
Chemistry
and Physics
Discussions
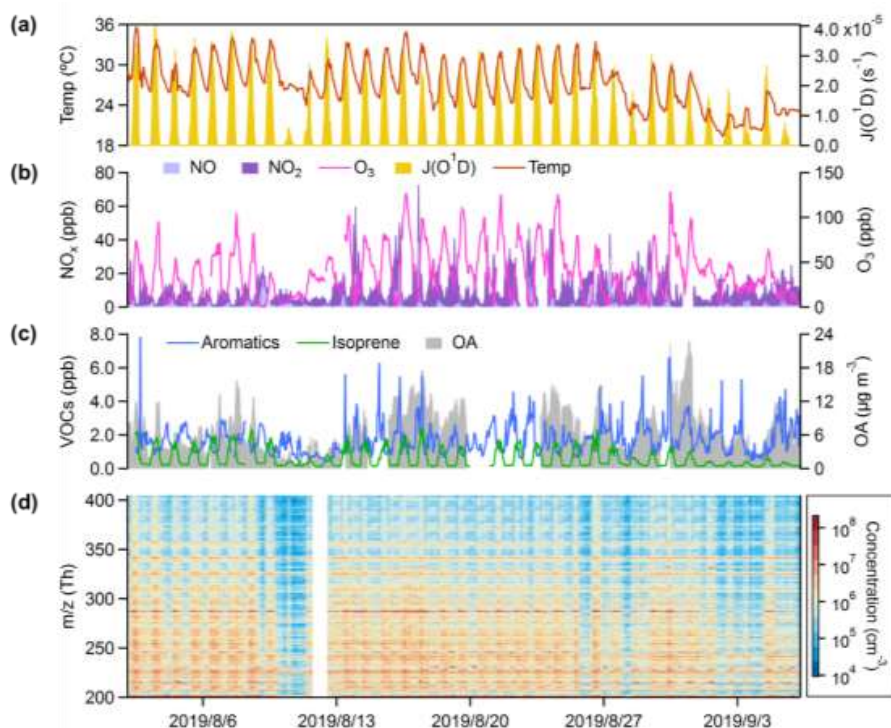
Figure 1. Overview of the observation. Time series of (a) temperature (Temp) and the photolysis frequency of O_3 (JO^1D), (b) O_3 and NO_x ($NO+NO_2$), (c) total aromatics (benzene + toluene + C_8 aromatics + C_9 aromatics + C_{10} aromatics + styrene), isoprene, and OA, and (d) mass spectra of nitrate CI-APi-TOF with m/z in the range of 202-404 Th.

The binPMF analysis was performed to characterize the sources or processes of OOMs. A 14-factor solution was selected to interpret the data set, including 3 factors about AVOCs daytime chemistry, 3 isoprene-related factors, 3 factors about BVOCs nighttime chemistry, 3 factors about nitrated phenols (NP), and 2 factors excluded from the following discussion. One of these two disregarded factors is mainly composed of fluorinated contaminations (F-contaminations), and the other is mainly a mixture of nitrated phenols and fluorinated contaminations (Mixed contaminations). When naming these factors, we prioritize the description of dominated species or their precursors, but if the precursors are complex mixtures, our naming highlights the characteristics of the chemical processes that drive certain factors. Although this may not be the optimal PMF solution, it still separates a lot of useful information. We also stress that the urban OOMs mix is unlikely to be a perfect combination of independent, unchanging factors, which is an underlying assumption in the PMF algorithm. As such, there will be no solution which is complete and perfect, but we chose a solution from which we were able to provide us with interesting insights. Details of the PMF diagnostics is provided in section S1 in the supplement. For the convenience of

Atmospheric
Chemistry
and Physics
Discussions

Open Access
EGU

272 discussions, we have grouped these factors. The factors in each group follow a similar
273 but not entirely exact pattern.
274
275 Table 1. Summary of molecular characteristics of 9 discussed non-nitrated-phenols
276 factors. The calculation of the relevant parameters is given in section S2 in
277 the supplement. Major peaks of each factor are summarized in section S3 in
278 the supplement.

Factor	Average concentration (cm-3)	Effective formulae	MW (g mol^{-1})	OSc	O:C	N:C	DBE	$\log_{10}(C^{*}(\mu g\ m^{-3}))$ in 300K
Aro-OOMs	1.86E+07	$C_{9.1}H_{14.3}O_{6.1}N_{0.6}$	230.2	-0.52	0.73	0.08	2.6	-1.7
Temp-related	4.50E+07	$C_{6.8}H_{10.2}O_{6.0}N_{0.5}$	195.8	-0.02	0.95	0.08	2.5	-1.4
Aliph-OOMs	2.11E+07	$C_{7.5}H_{12.2}O_{6.7}N_{1.2}$	225.7	-0.55	0.96	0.17	1.9	0.0
Photo-related	4.77E+07	$C_{6.9}H_{11.0}O_{7.4}N_{1.2}$	228.3	-0.28	1.18	0.20	1.8	-1.1
O_x & SOA-related	2.59E+07	$C_{6.6}H_{9.8}O_{6.8}N_{1.1}$	214.2	-0.24	1.11	0.19	2.2	-0.3
Isop-OOMs	2.83E+07	$C_{5.5}H_{9.6}O_{6.9}N_{1.4}$	205.8	-0.51	1.34	0.28	0.9	1.2
BVOCs-OOMs I	1.68E+07	$C_{7.2}H_{11.5}O_{7.0}N_{1.0}$	224.1	-0.26	1.06	0.16	2.0	-1.4
BVOCs-OOMs II	9.05E+06	$C_{9.2}H_{14.6}O_{7.1}N_{0.9}$	251.3	-0.45	0.83	0.11	2.5	-2.8
BVOCs-OOMs III	1.57E+07	$C_{8.6}H_{13.7}O_{6.9}N_{1.2}$	243.3	-0.64	0.87	0.16	2.1	-0.7

279 Note: MW is the molecular weight, OSc is the carbon oxidation state, O:C is the oxygen
280 to carbon ratio, N:C is the nitrogen to carbon ratio, DBE is the double bond equivalent,
281 C^{*} the saturation concentration and $\log_{10}(C^{*})$ is the volatility.
282
283
284 **3.1 AVOCs daytime chemistry**
285
286 The following daytime factors are characterized by C_6-C_9 OOMs (Fig. 2(a)), considered
287 to be derived from the oxidation of anthropogenic VOCs in this urban atmosphere,
288 while we cannot completely exclude the present of BVOCs-derived OOMs, such as C_5
289 and C_{10} OOMs.
290

Atmospheric
Chemistry
and Physics
Discussions
Open Access
EGU
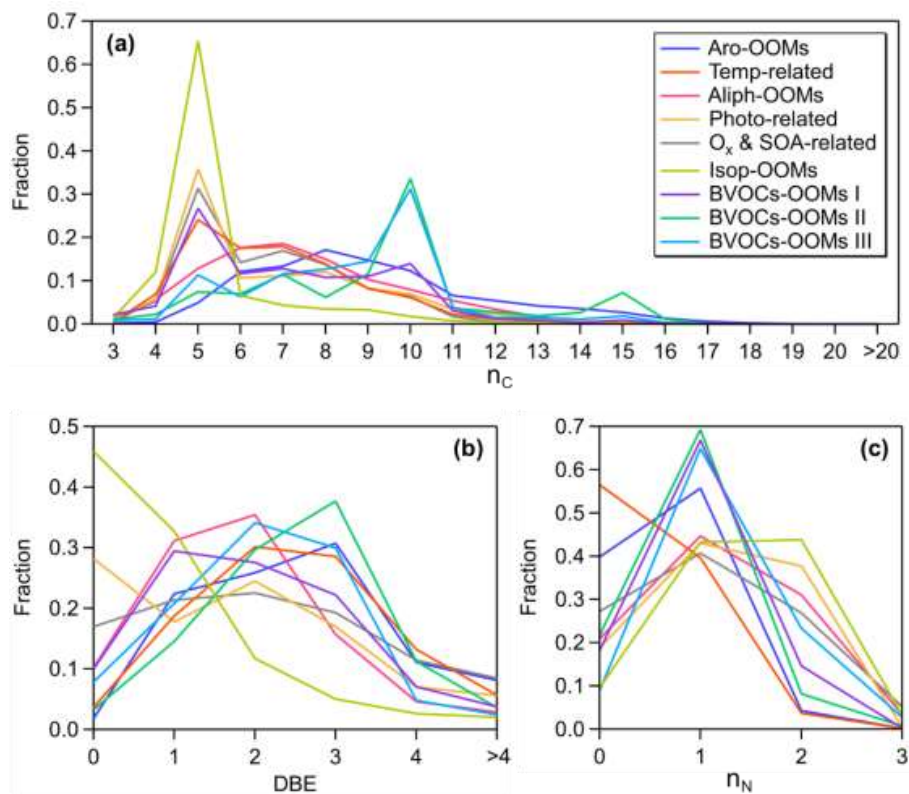
291 Figure 2. The distributions of observed non-nitro OOMs grouped by (a) the number of
292 carbon atoms (n_C), (b) DBE, and (c) the number of nitrogen atoms (n_N) in 9 factors.
293 Since the signals of RO$_2$ are very weak, RO$_2$ from BVOCs OOMs I and BVOCs OOMs
294 II are excluded in (b) to keep the integer value of DBE.
295

Aro-OOMs factor

300 The effective DBE of this factor is the largest among all factors (Table 1), with main
301 signals come from compounds with DBE > 2 (Fig. 2(b)) and consistent with the nature
302 of the oxidation products of aromatics (Fig. 3(a)). Combined with the correlation with
303 the production rates of OH-initiated primary peroxy radicals (RO$_2$) from aromatics
304 calculated by Eq. (3) (Fig. 4), this factor is supposedly dominated by aromatics-derived
305 OOMs (Aro-OOMs). The Aro-OOMs factor increases from 5:00 LT with a maximum
306 at 10:00 LT and a sub peak around 16:00 LT (Fig. 3(e)), following the diurnal variations
307 of P_{RO2} of C$_7$-C$_{10}$ aromatics (Fig. 4(b-d)) but poorly correlated with P_{RO2} of benzene
308 (Fig. 4(a)). Furthermore, OOMs with 8 carbon atoms have the highest signal in this
309 factor (Fig. 2(a)), derived from the most abundant C$_8$-aromatics + styrene RO$_2$ (Fig.
310 4(f)). Both of these can be explained by the fact that substituted aromatics have higher
311 OH reactivity (Bloss et al., 2005) and higher HOM yields (Wang et al., 2017;Molteni

312 et al., 2018) than their homologues with less carbon atoms. In terms of molecular

313 formula, the aromatics-derived OOMs have an overlap with monoterpenes-derived

314 OOMs (Mehra et al., 2020). Monoterpenes can contribute more C_{10} OOMs than

315 aromatics ($P_{MT-RO_2} > P_{C_{10}\ Aro-RO_2}$), but aromatics play a more important role in total

316 in this factor since they provide more RO_2 in the urban atmosphere (Fig. 3(f)).

317

318 $$P_{RO_2} = \ k_{OH+VOC} \bullet [OH] \bullet [VOC] \qquad (3)$$

319
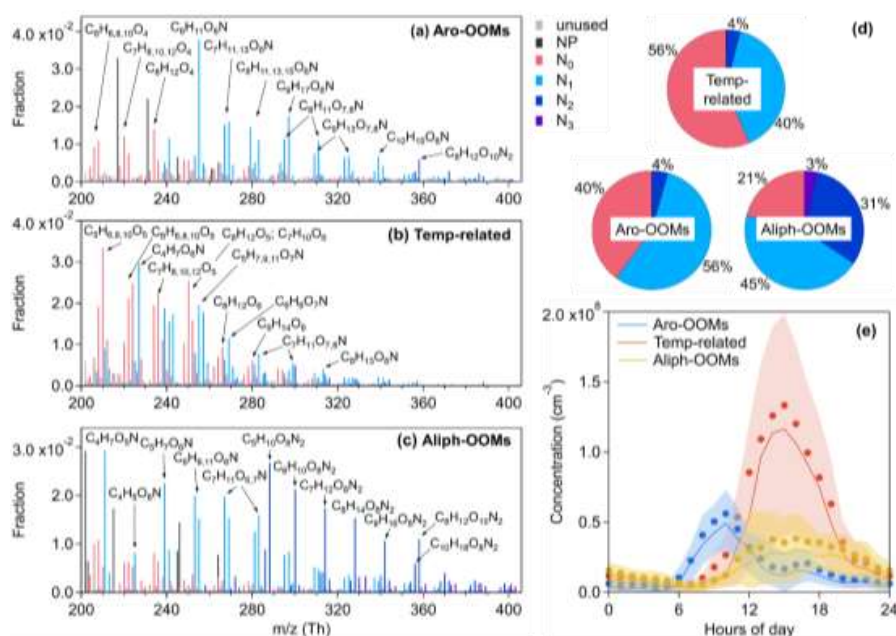
320

321 Figure 3. Mass spectra of (a) the Aro-OOMs factor, (b) the Temp-related factor, (c) the

322 Aliph-OOMs factor, and the elemental formulas of major peaks are labeled above them.

323 Peaks are color-coded by n_N as indicated at the top right of the figure, and the fractions

324 of peaks grouped by n_N are reported in (d) the pie chart. The gray sticks are fluorinated

325 contaminations, or non-identified compounds. The nitrated phenols are drawn

326 separately with black peaks in (a), (b) and (c), and were not included in (d). So n_N can

327 more reliably represent the number of nitrate groups in each molecule. Diurnal patterns

328 (Beijing time) of these three factors are shown in (e), the bold solid lines are the median

329 values, shaded areas represent percentiles of 75 % and 25 % and solid circles represent

330 mean values.

331

332 The main molecules of the Aro-OOMs factor are summarized in Table S2. The $C_xH_{2x-5}O_6N$

333 (x=6-12, of which $C_8H_{11}O_6N$ is the most intense) series can be produced by the

334 reaction (R1a) of NO with the bicyclic peroxy radicals (HO-Ar-$(O_2)_2$), the key

335 intermediates for aromatics oxidation proposed in the MCM (Bloss et al., 2005;Birdsall

336 and Elrod, 2011). And here dihydroxy nitro-BTEX ($C_xH_{2x-7}O_4N$, x=6-8) can be treated

337 as indicators of aromatics oxidation. In addition to the conventional products, $C_9H_{13}O_{7-}$
338 $_9N$ from the $C_xH_{2x-5}O_{7-9}N$ (x=7-13) series are also significant in the OH-initiated and
339 NO$_x$-influenced oxidation experiments of 1,2,4-trimethylbenzene   (Zaytsev et al.,
340 2019) and of 1,3,5-trimethylbenzene (Tsiligiannis et al., 2019). More oxygenated
341 compounds may come from auto-oxidation and multigenerational OH attacks. However,
342 the effective OSc of this factor (Table 1) is lower than that of oxidation products of
343 aromatics in recent laboratories (Zaytsev et al., 2019;Tsiligiannis et al., 2019;Garmash
344 et al., 2020;Wang et al., 2020c). We speculate that the abundances of NO$_x$ relative to
345 oxidants and precursors in these experiments are not sufficient to reproduce the
346 atmospheric conditions during our observation, or that HOMs are more concentrated in
347 aerosols due to the large condensation sink on this site (Qi et al., 2015). Although
348 species with DBE < 3 (Fig. 2(b)) in this factor are most likely produced from multiple
349 OH attacks in aromatics oxidation, we can't rule out the contribution of alkanes co-
350 emitted with aromatics, such as the series $C_xH_{2x-1}O_6N$ (x=5-14).
351
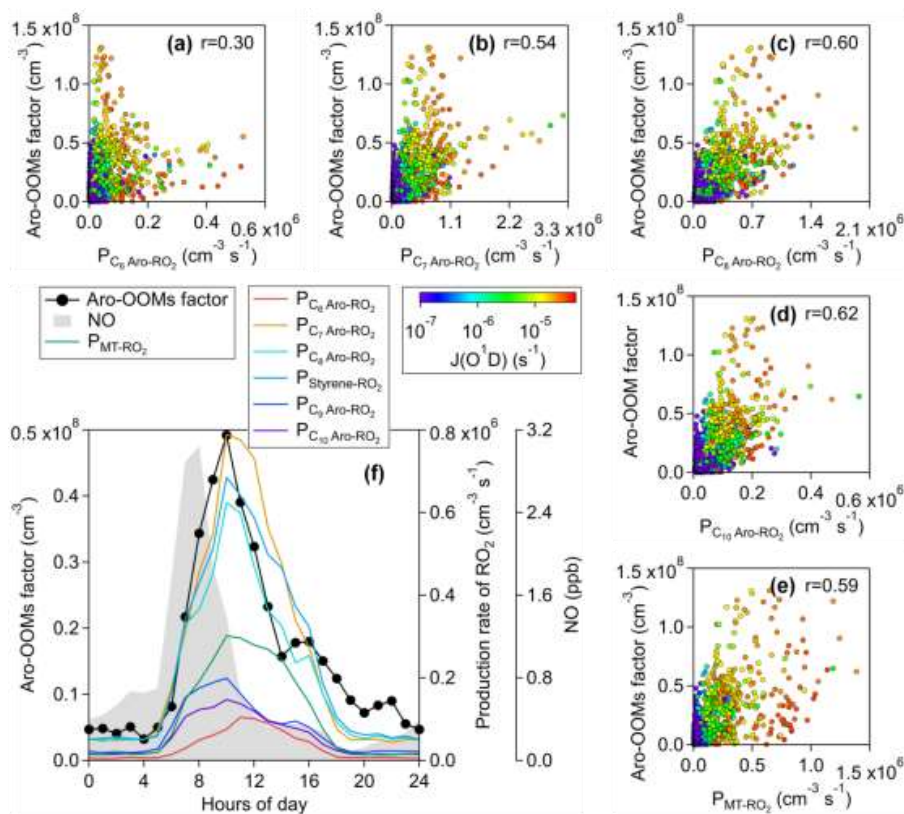
352
353 Figure 4. Correlations of the Aro-OOMs dominated factor with production rate of RO$_2$
354 from OH-initiated oxidation of (a) benzene ($P_{C_6\ Aro-RO_2}$), (b) toluene ($P_{C_7\ Aro-RO_2}$), (c)
355 C_8 aromatics ($P_{C_8\ Aro-RO_2}$), (d) C_{10} aromatics ($P_{C_{10}\ Aro-RO_2}$), and (e) Monoterpenes

356 (P_{MT-RO_2}). All the scatters are colored by J(O^{1}D), to show the difference between day
357 and night. The median diurnal patterns of this factor and related parameters are plotted
358 in (f).

359

360 **Temp-related factor**

361

362 This factor is named due to good correlation with temperature (Fig. 5), and shows
363 maximum intensity in the afternoon around 15:00 (Fig. 3(e)). The Temp-related factor
364 is the only one dominated by non-nitrogenous organics (Fig. 3(b) and (d)), and has the
365 highest effective OSc (Table 1) among all the factors. The $C_xH_{2x-4}O_5$ (x=5-11,
366 summarized in Table S3), $C_xH_{2x-2}O_5$ (x=5-10), $C_xH_{2x-6}O_5$ (x=5-11), and $C_xH_{2x-4}O_6$
367 (x=5-10) series are possibly products from RO$_2$ terminated by HO$_2$ (R2a), or closed-
368 shell products from RO in reactions R3a or R3b. Temperature starts to rise at 6:00 LT
369 (Fig. 12(b)), but this factor does not accumulate significantly until after about 10:00 LT
370 (Fig. 3(e)), when the mixed level of NO is reduced to 1 ppb (Fig. 4(f)). This
371 phenomenon suggests a probability of HO$_2$-driven chemistry of this factor under low
372 NO conditions, since that NO can consume HO$_2$ and compete with HO$_2$ for RO$_2$. Such
373 low-NO atmospheric oxidation pathways have been suggested to be non-negligible in
374 the afternoon in central Beijing (Newland et al., 2021).

375

376 A factor caused by similar chemical processes called isoprene afternoon was discovered
377 in the nitrate CI-APi-TOF data collected at a forest site in Centreville, Alabama, USA
378 (Massoli et al., 2018), correlated well with HO$_2$, O$_3$, and temperature. We also observed
379 a number of isoprene oxidation products in the Temp-related factor (nC = 4, 5 in Fig.
380 2(a)). Many of the $C_xH_{2x-1}O_6N$ (x=3-7) and $C_xH_{2x-3}O_6N$ (x=4-9) series were also present
381 in the light HOMs factor which was supposed to be fragments from the oxidation of
382 larger VOCs (e.g., monoterpene) in Hyytiälä, Finland (Yan et al., 2016). While at the
383 SORPES station, the C$_6$-C$_9$ ions should mainly come from the oxidation of
384 anthropogenic VOCs. At lower temperatures, the propensity of condensable organic
385 molecules to condense into aerosol makes the concentration measured using nitrate CI-
386 APi-TOF lower. Thus, the total concentration of the Temp-related factor in the gas and
387 aerosol phases was calculated based on gas-particle equilibrium (section S4 in
388 the supplement), and was found to be still temperature dependent (Fig. S6), illustrating
389 the temperature-influenced chemical process controlling the factor. For instance,
390 Unimolecular reaction rates like RO$_2$ H-shifts increase qualitatively with temperature
391 (Bianchi et al., 2019;Frege et al., 2018).

392

393 $$RO_2\bullet \ + \ NO \ \rightarrow \ RONO_2 \qquad (R1a)$$
394 $$RO_2\bullet \ + \ NO \ \rightarrow \ RO\bullet \ + \ NO_2 \qquad (R1b)$$
395 $$RO_2\bullet \ + \ HO_2\bullet \ \rightarrow \ ROOH + \ O_2 \qquad (R2a)$$
396 $$RO_2\bullet \ + \ HO_2\bullet \ \rightarrow \ RO\bullet \ +\bullet OH + \ O_2 \qquad (R2b)$$
397 $$RO\bullet \ + \ O_2 \ \rightarrow \ RC=O \ + \ HO_2\bullet \qquad (R3a)$$
398 $$RO\bullet \ + \ O_2 \ \rightarrow \ fragments \qquad (R3b)$$

399

400

401
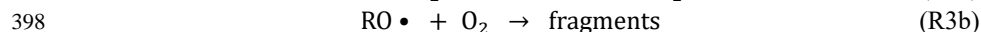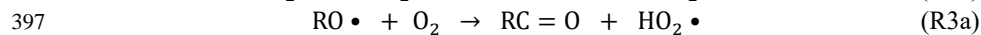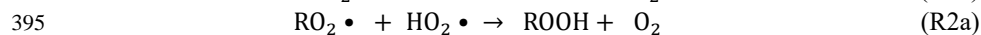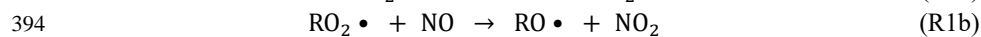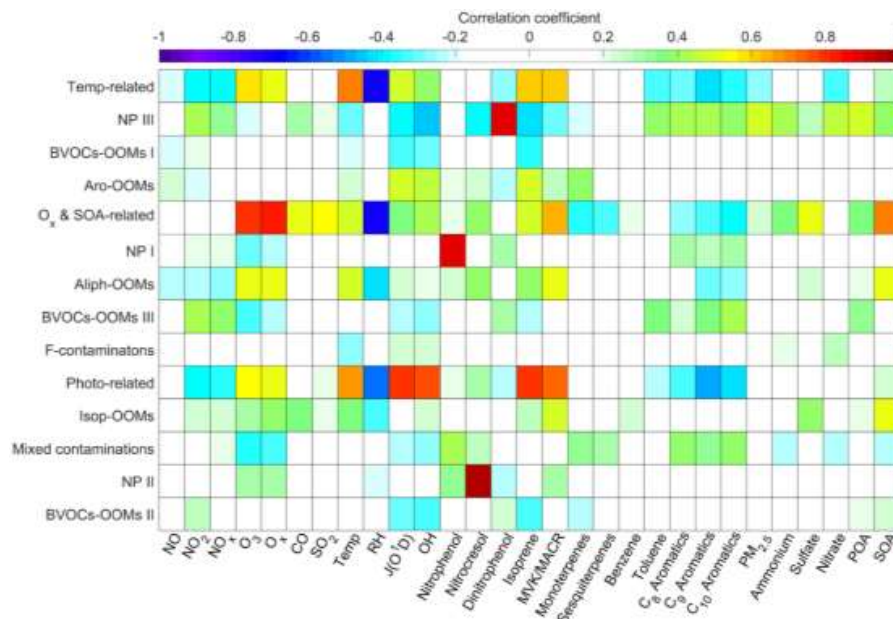
Figure 5. Correlations of PMF factors with external gas-phase and particulate tracers from other instruments deployed at the SOPRES station, with the color representing the Pearson correlation coefficients. From left to right, the tracers are gas-phase species (NO, NO$_2$, NO$_x$, O$_3$, CO, SO$_2$), meteorological data (temperature (Temp), relative humidity (RH), photolysis constants (J(O^{1}D))), nitrate CI-APi-TOF data (OH, nitrophenol, nitrocresol, dinitrophenol), PTR-ToF-MS data (isoprene, methyl vinyl ketone/methacrolein (MVK/MACR)), monoterpenes, sesquiterpenes, benzene, toluene, C$_8$ aromatics, C$_9$ aromatics, C$_{10}$ aromatics), PM$_{2.5}$, and ACSM data (ammonium, sulfate, nitrate, POA, SOA).

Aliph-OOMs factor

This factor is dominated by organic nitrates (Fig. 3(c) and (d)), and contains the bulk of anthropogenic di-nitrates and tri-nitrates. The C$_x$H$_{2x-2}$O$_8$N$_2$ (x=4-13, summarized in Table S3) and C$_x$H$_{2x}$O$_8$N$_2$ (x=4-9) series have not been reported in aromatics oxidation experiments under high NO$_x$ conditions (Tsiligiannis et al., 2019;Wang et al., 2020c), and nor in the forest or rural environments (Yan et al., 2016;Massoli et al., 2018). A reasonable assumption is that these saturated or nearly saturated compounds are the products of aliphatics (including alkanes, alkenes, aliphatic alcohol, etc.) during their oxidation affected intensively by NO$_x$ in the urban atmosphere. The Aliph-OOMs factor has a broad afternoon peak lasting from 14:00 to 19:00 LT (Fig. 3(e)), suggesting that the formation of multi-nitrate requires enough OH exposure time.

Considering a simple scenario of alkane photo-oxidation under high NO$_x$ conditions:

426 the RO_2 generated from OH attack is completely terminated by NO (Fig. 6(a)). The
427 chain-retaining products are $C_nH_{2n}O$ (one more carbonyl group than the precursor) and
428 $C_nH_{2n+1}O_3N$ (one more nitrate group than the precursor), and the re-oxidation of these
429 products is a repetition of the above process which is defined as the basic reaction
430 scheme. The multiple (1st to 3rd) generation products of alkanes summarized in Fig.
431 6(b) are regarded as reference compounds, which we compare OOMs with to
432 investigate other mechanisms that differ from those shown in Fig. 6(a). Specifically,
433 this comparison is performed between the reference molecule and OOMs with the same
434 numbers of carbon, hydrogen and nitrogen atoms, but different numbers of oxygen

435 atoms. The number of extra oxygen ($n_{O_{extra}}$) from each aliphatic OOM over its

436 corresponding reference molecule was calculated by Eq. (4), that is, subtracting

437 carbonyl and nitrate oxygens from the molecule. Thus, the $n_{O_{extra}}$ can represent the

438 additional oxygenated moieties such as hydroxyl group (-OH), peroxy group (-OOH),
439 and possibly ether group. These functional groups may come from RO isomerization
440 (Orlando et al., 2003), the addition of OH to alkenes, or pre-existing moieties in the
441 precursor, RO_2 autoxidation or specific RO_2 bimolecular termination reactions
442 (RO_2+RO_2, RO_2+HO_2).
443

444 $$n_{O_{extra}} = n_O - DBE - 3 \times n_N \qquad (4)$$

445

446 As showed in Fig. 6(c), aliphatic OOMs in this factor are mainly the third-generation
447 products followed by the second-generation products, and both of which have one or
448 two oxygen-containing functional groups in addition to the carbonyls and nitrates. It
449 should be noted that the first-generation (Fig. 6(a)) and basic products (Fig. 6(b)) here
450 are underestimated due to the low sensitivity of nitrate CI-APi-TOF to these compounds.
451 The multifunctional products of aliphatics are condensable to form SOA (correlation
452 coefficients with SOA showed in Fig. 5). Recent work has showed that autoxidation is
453 more common than previously thought (Wang et al., 2021), and more studies are needed
454 to explore the oxidation mechanisms of anthropogenic aliphatics and to evaluate their
455 contribution to SOA.
456
457
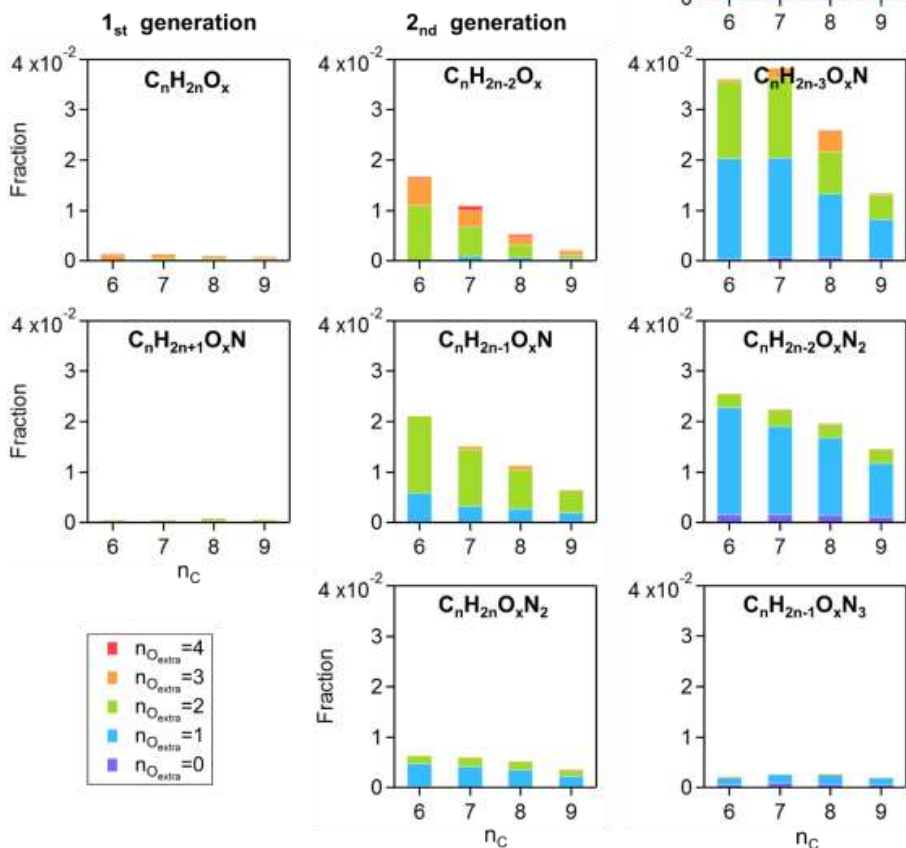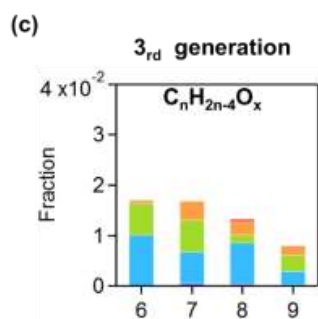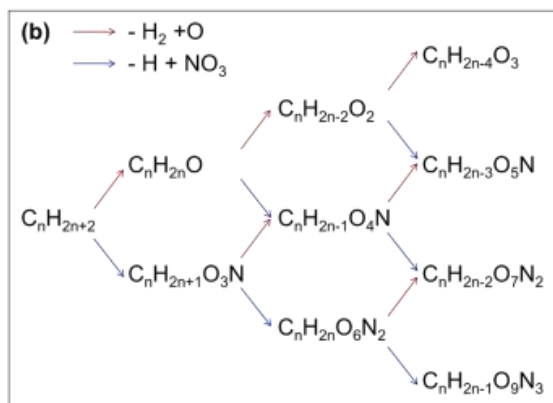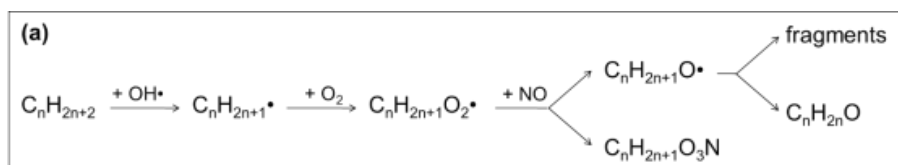
459 Figure 6. (a) Simplified oxidation mechanism for alkanes attacked by OH once under
460 NO$_x$-controlled conditions. (b) summarizes the changes in molecular formula of the 1st
461 to 3rd generation products of alkanes, based on the basic reaction scheme in (a). (c)
462 shows the fraction of potential alkanes-derived compounds in the Aliph-OOMs factor.
463 The compounds listed in (c) are grouped according to the molecular formulas in (b),
464 i.e., the same number of carbon, hydrogen and nitrogen atoms, but different numbers
465 of oxygen atoms. The bars in (c) are colored with $n_{O_{extra}}$. Please see text for details
466 about $n_{O_{extra}}$.

467
468 **3.2 Isoprene-related chemistry**
469
470 The following factors are characterized by C$_5$ OOMs (Fig. 2(a)), of which an isoprene
471 dihydroxyl dinitrate C$_5$H$_{10}$O$_8$N$_2$ (charged by NO$_3^-$ at m/z 288 Th) is the fingerprint
472 molecule (Fig. 7). Apart from isoprene-derived compounds, OOMs formed from other
473 precursors undergoing the similar chemical processes are also allocated to these three
474 factors.

475
476 **Photo-related factor**
477
478 This factor is defined based on its correlation with J(O^{1}D) (Fig. 5), having an apparent
479 diurnal cycle with a peak at 12:00 LT (Fig. 7(e)). The major peak of the Photo-related
480 factor is C$_5$H$_{10}$O$_8$N$_2$ (Fig. 7(a)), most probably generating from double OH attack
481 proceed with double RO$_2$+NO termination (Jenkin et al., 2015). C$_5$H$_{10}$O$_8$N$_2$ can be also
482 produced in NO$_3$+ isoprene system (Ng et al., 2008;Zhao et al., 2020), whereas in this
483 study, the nocturnal C$_5$H$_{10}$O$_8$N$_2$ is principally from the Isop-OOMs factor (Fig. 8(b))
484 which will be discussed later. Other peaks with nC≤5, like C$_5$H$_7$O$_7$N, C$_4$H$_7$O$_6$N,
485 C$_5$H$_9$O$_6$N, are also likely to be the isoprene products. The total signal of compounds
486 with nC > 5 is not low, although their respective proportions are not as prominent as C$_5$
487 species (Fig. 7(d)), implying the contribution of other precursors together with isoprene.
488 In addition, the relationship of this factor with isoprene and J(O^{1}D) together (Fig. 5)
489 reveals the effect of light-dependent emission of isoprene on it.

490
491 **O$_x$ & SOA-related factor**
492
493 The atmospheric oxidation of VOCs produces low-volatile compounds, forming SOA
494 through gas-particle partitioning, and concurrently promotes ozone formation
495 (Atkinson, 2000). Both SOA and O$_x$ have long lifetimes (>12 h), and their correlations
496 have been extensively investigated (Herndon et al., 2008;Wood et al., 2010;Hu et al.,
497 2016). The OOMs factor related to ozone and SOA together (Fig. 5), having slightly
498 elevated concentrations during daytime (Fig. 7(e)), is considered to be generated from
499 this photochemical aging process. Apart from C$_5$H$_{10}$O$_8$N$_2$, other isoprene multi-nitrates
500 are also present in this factor. C$_5$H$_9$O$_{10}$N$_3$, an isoprene hydroxyl trinitrate requiring at

Atmospheric
Chemistry
and Physics
Discussions
Open Access
EGU

501 least two steps of oxidation found in the experimental study on isoprene oxidation by
502 NO3 (Zhao et al., 2020), naturally does not appear in the photo-related factor at all, but
503 is mostly apportioned into the O_x & SOA-related factor and the Isop-OOMs factor (Fig.
504 8(c) and 8(d)). Like the photo-related factor, isoprene is a significant but not the only
505 precursor of this factor (Fig. 2 and 7). The biggest peak of the O_x & SOA-related factor
506 is an ion at m/z 264 with formula $C_6H_5O_3N$ ($HNO_3NO_3^-$), identified as an adduct of
507 nitrophenol ($C_6H_5O_3N$) with nitrate dimmer ($HNO_3NO_3^-$). The time variation of
508 $C_6H_5O_3N$ ($HNO_3NO_3^-$) is influenced by the reagent ions in addition to the atmospheric
509 nitrophenol. So far, we don't know why this compound share the same processes with
510 others, but we did a test that removing the bins with unit m/z = 264 from the input
511 matrix and still got this factor from PMF model.
512
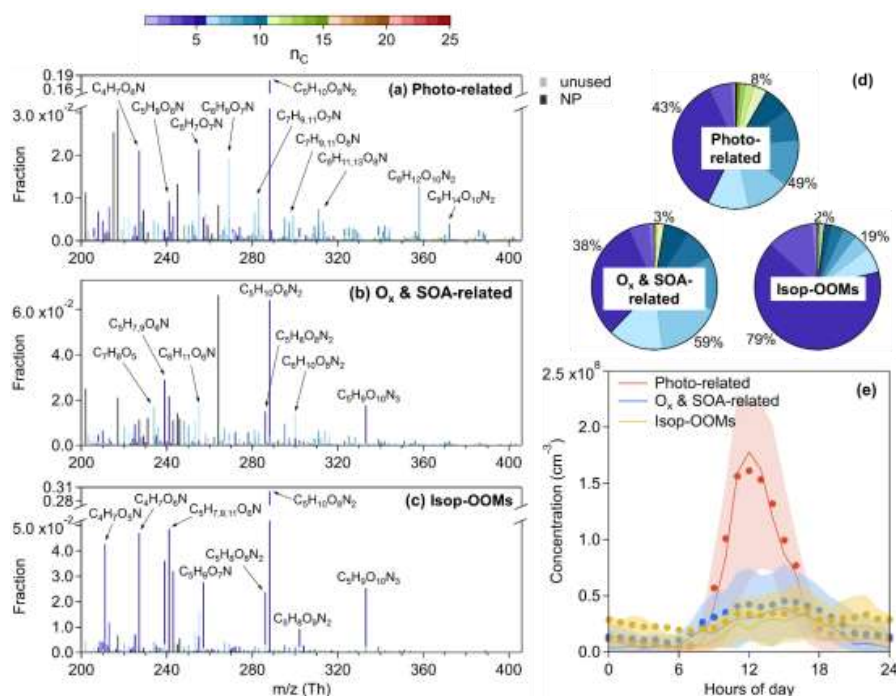
513
514 Figure 7. Mass spectra of (a) the Photo-related factor, (b) the O_x & SOA-related factor,
515 (c) the Isop-OOMs factor, and the elemental formulas of major peaks are labeled above
516 them. Peaks are color-coded by n_C as indicated at the top of the figure, and the fractions
517 of peaks grouped by n_C are reported in (d) the pie chart. The gray sticks are fluorinated
518 contaminations, or non-identified compounds. The nitrated phenols are drawn
519 separately with black peaks in (a), (b) and (c). The molecules represented by the gray
520 and black sticks were not included in (d). Diurnal patterns of the three factors are shown
521 in (e), the bold solid lines are the median values, shaded areas represent percentiles of
522 75 % and 25 % and solid circles represent mean values.
523
524 **Isop-OOMs factor**

525

526 The mass spectra of the Isop-OOMs factor, as its name implies, is exclusively
527 contributed by isoprene-derived compounds (Fig. 7(c)). $C_5H_{10}N_2O_8$ contributes about
528 30% of the intensity of this factor, and the dominance of $C_5H_{10}N_2O_8$ was also found in
529 the isoprene nitrates type I factor in Centreville (Massoli et al., 2018). In addition to
530 multi-nitrates ($C_5H_{10}O_{7-8}N_2$, $C_5H_8O_{6-9}N_2$, and $C_5H_9O_{10}N_3$ summarized in Table. S6),
531 several mononitrate series ($C_4H_7O_{5-7}N$, $C_5H_9O_{4-9}N$, $C_5H_7O_{5-8}N$, and $C_5H_{11}O_{5-6}N$) of
532 this factor are also abundant in the isoprene nitrates type II factor in Centreville
533 (Massoli et al., 2018). Many of isoprene nitrates here have been specially investigated
534 in our previous observations in the YRD (Xu et al., 2021), and have been discovered in
535 other filed measurements (Lee et al., 2016;Massoli et al., 2018) and in many
536 laboratories (Ng et al., 2008;Lambe et al., 2017). Generally, these compounds are
537 second- and third-generation OH oxidation products of isoprene under high-NO_x
538 conditions (Wennberg et al., 2018).

539

540 The diurnal pattern of the Isop-OOMs factor is relatively unclear (Fig. 7(e)), with
541 obvious differences between mean and median values usually caused by plume events.
542 This indicates that isoprene chemistry, usually varying evidently from day (OH-
543 initiated) to night (NO_3-initiated), is not the driver of this factor. This factor correlates
544 positively with MVK / MACR and SOA (r>0.50, showed in Fig. 5), but not with
545 isoprene and OH. It seems that these isoprene OOMs are produced elsewhere and then
546 transported due to their longer lifetime determined by their relatively high volatility
547 (Table 1). The Isop-OOMs factor in the continental air masses are more intensive than
548 those in the coastal and YRD air masses (Fig. S7), consistent with the spatial
549 distribution of isoprene emissions (Sindelarova et al., 2014). An archetypal episode
550 affected by continental air masses (August 13 to August 17, 2019) is showed in Fig. 8.
551 During this period, $C_5H_9O_{10}N_3$ was almost entirely transported, while $C_5H_{10}O_8N_2$ has
552 strong in situ photochemical generation, in addition to the source of transport.

553

554
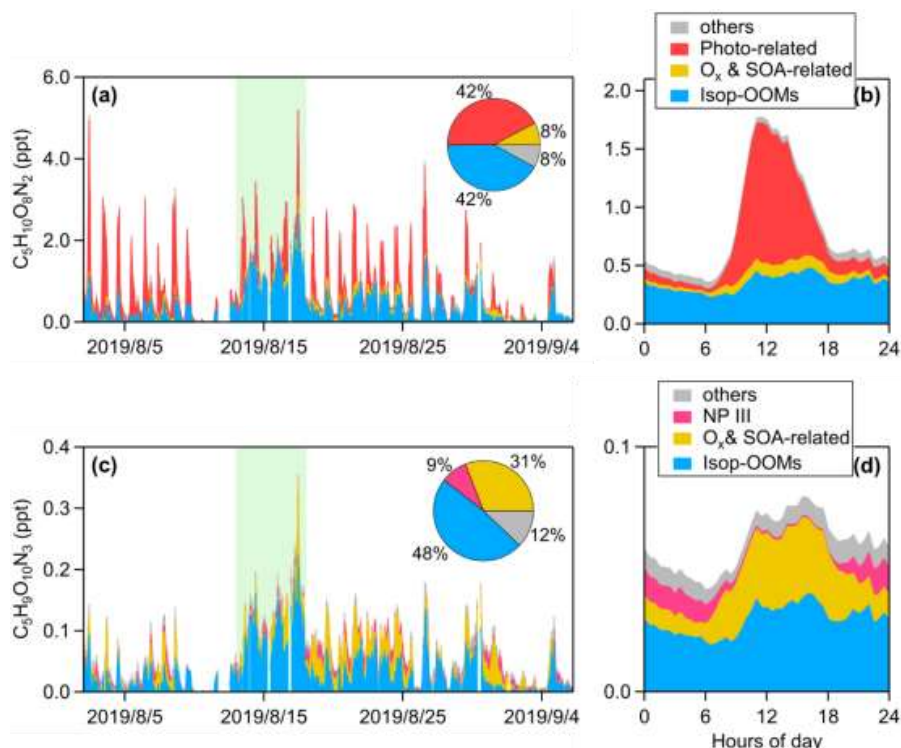
Figure 8. Stacked (a) time series and (b) mean diurnal pattern of isoprene dihydroxyl dinitrate ($C_5H_{10}O_8N_2$). Stacked (c) time series and (d) mean diurnal pattern of isoprene hydroxyl trinitrate ($C_5H_9O_{10}N_3$). The contribution ratios of each PMF factor to these two compounds are reported in the pie chart respectively. The light green shaded area represents a typical episode influenced by transported continental air masses (August 13 to August 17, 2019).

3.3 BVOCs nighttime chemistry

The following nighttime factors are characterized by C_{10} OOMs (Fig. 2(a)), which are identified as the oxidation products of monoterpenes. Except for the BVOCs-OOMs I factor (Fig. 9(a)), the contribution of isoprene-derived OOMs was much lower in these factors. Compared to the above isoprene-related factors, $C_5H_{10}O_8N_2$ and $C_5H_9O_{10}N_3$ was no longer significantly present in the following factors.

BVOCs-OOMs I factor

The first nighttime factor has its maximum concentration at around 20:00 LT, and decreases to very low value during the day. It is moderately correlated with the production rate of NO_3 radical (P_{NO3} derived from Eq. 5) at night, and reaches high intensity only under conditions of NO below 1 ppb (Fig. 10(a)), indicating a chemical

576 process of NO$_3$ radical. The concentration of this factor is mainly from C$_5$ peaks,
577 followed by C$_6$-C$_{10}$ peaks (Fig. 9(d)), about 80% of which are ONs (Fig. 2(c)),
578 designating the oxidations of isoprene and monoterpenes by NO$_3$ (BVOCs-OOMs I).
579 In the case of isoprene oxidation, the nitrate groups of C$_5$H$_9$O$_{4-8}$N, C$_5$H$_7$O$_{5-8}$N and
580 C$_4$H$_7$O$_{5-6}$N series (summarized in Table S8) are likely to come from the addition of NO$_3$.
581 Next, the C$_5$H$_{10}$O$_{8-9}$N$_2$ and C$_5$H$_8$O$_{7-10}$N$_2$ series are probably second-generation products.
582 These compounds derived from isoprene+NO$_3$ system have been discussed in previous
583 laboratory (Kwan et al., 2012;Zhao et al., 2020) and ambient data sets (Ayres et al.,
584 2015;Xiong et al., 2015). Additionally, The C$_6$-C$_{10}$ species are potentially the products
585 of monoterpenes degraded by NO$_3$.

586

587 $$P_{NO_3} = k_{NO_2+O_3} \bullet [NO_2] \bullet [O_3] \tag{5}$$

588
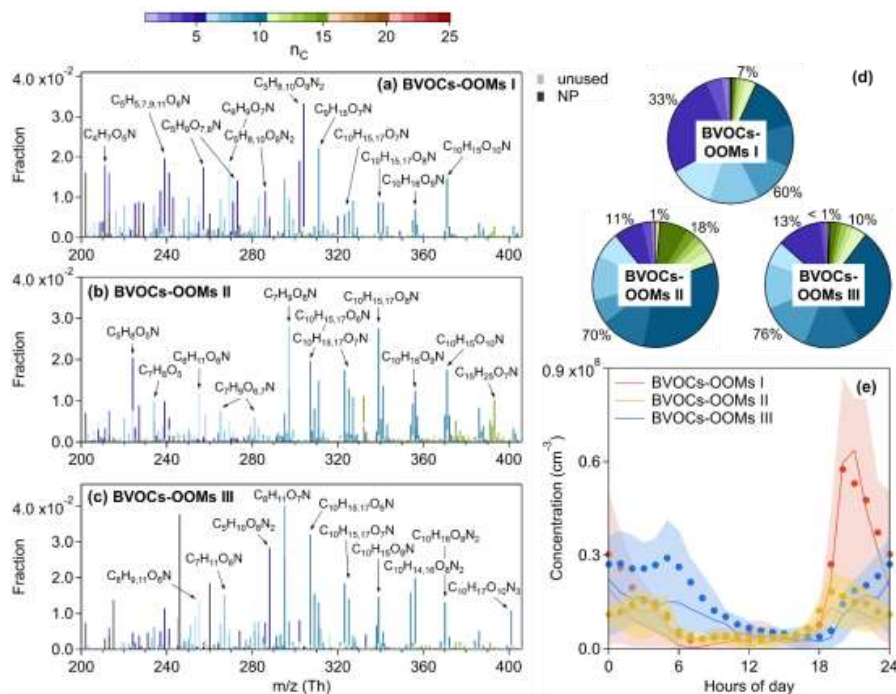
589

590 Figure 9. Mass spectra of (a) the BVOCs-OOMs I factor, (b) the BVOCs-OOMs II
591 factor, (c) the BVOCs-OOMs III factor, and the elemental formulas of major peaks are
592 labeled above them. Peaks are color-coded by n$_C$ as indicated at the top of the figure,
593 and the fractions of peaks grouped by n$_C$ are reported in (d) the pie chart. The gray
594 sticks are fluorinated contaminations, or non-identified compounds. The nitrated
595 phenols are drawn separately with black peaks in (a), (b) and (c). The molecules
596 represented by the gray and black sticks were not included in (d). Diurnal patterns of
597 these three factors are shown in (e), the bold solid lines are the median values, shaded
598 areas represent percentiles of 75 % and 25 % and solid circles represent mean values.

Atmospheric
Chemistry
and Physics
Discussions
Open Access

EGU

599

600 **BVOCs-OOMs II factor**

601

602 The second nighttime factor are intense at night and over five times lower during the
603 day. Like the BVOCs-OOMs I factor, this factor has high concentrations when NO is
604 reduced leading to increased NO_3 availability (Fig. 10(b)), and about 80% of
605 compounds in this factor are ONs (Fig. 2 (c)). Accordingly, this may also be a factor
606 strongly influenced by NO_3. It is dominated by C_6-C_{10} OOMs, among which the highest
607 intensity is at C_{10} (Fig. 9(d)), coherent with the nature of monoterpene products
608 (BVOCs-OOMs II). This factor has weaker signals at C_{15} which are plausibly the
609 products of sesquiterpenes but could also be dimmers formed from R4 (monoterpenes
610 + isoprene or monoterpenes + C_5 monoterpenes fragments). Compared to the BVOCs
611 OOMs I factor (Fig. 9(d)), this factor has more large mass molecules (C_{10}) and fewer
612 small mass molecules (C_5), resulting in an effective volatility over one order of
613 magnitude lower.   A NO_3-initiated factor, called the nighttime type-2 factor, has also
614 been discovered in Hyytiälä, Finland (Yan et al., 2016), but the similar factor we found
615 has a higher proportion of organic nitrates, due to the more abundant NO_x here.

616

617 $$RO_2 \bullet \ + \ R'O_2 \bullet \ \rightarrow \ ROOR' \ + \ O_2 \qquad\qquad (R4)$$

618

619 $$C_{10}H_{16} + NO_3 \bullet \ \overset{O_2}{\rightarrow} \ C_{10}H_{16}NO_5 \bullet \ \xrightarrow{H-shift+O_2} \ C_{10}H_{16}NO_7 \bullet$$

620 $$\xrightarrow{H-shift+O_2} \ C_{10}H_{16}NO_9 \bullet \ \xrightarrow{H-shift+O_2} \ C_{10}H_{16}NO_{11} \bullet$$

621 (R5a)

622

623 $$C_{10}H_{16} + NO_3 \bullet \ \overset{O_2}{\rightarrow} C_{10}H_{16}NO_5 \bullet \rightarrow \ C_{10}H_{16}NO_4 \bullet \ \ (Alkoxy)$$

624 $$\xrightarrow{H-shift+O_2} \ C_{10}H_{16}NO_6 \bullet \ \xrightarrow{H-shift+O_2} \ C_{10}H_{16}NO_8 \bullet$$
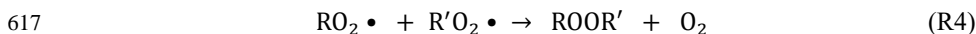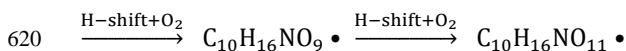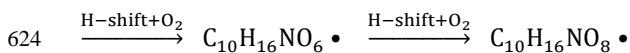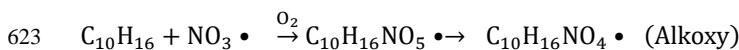
625 (R5b)

626

627 In terms of fingerprint molecules of this factor (summarized in Table S9), The
628 $C_{10}H_{15}O_{5-12}N$ series are carbonyl products from precursor RO_2 or RO terminations,
629 while the $C_{10}H_{17}O_{5-9}N$ series are alcohol or hydroperoxide products from precursor RO_2
630 terminations. The $C_7H_9O_{6-8}N$, $C_9H_{15}O_{6-9}N$, $C_9H_{13}O_{7-10}N$, and $C_8H_{13}O_{7-8}N$ series are
631 expected to be fragments. The closed-shell compounds mentioned above have been
632 reported in the experiments of monoterpenes + NO_3 system (Nah et al., 2016;Faxon et
633 al., 2018;Takeuchi and Ng, 2019).

634

635 It is noteworthy that a set of nitrogen-containing radicals, $C_{10}H_{16}O_{6-11}N$ (peak fitting
636 are shown in Fig. S8), is present in the BVOCs-OOMs II factor. Starting from a generic
637 monoterpene molecule with the formula $C_{10}H_{16}$, the NO_3 addition with fast O_2 addition
638 results in a peroxy radical with the formula $C_{10}H_{16}O_5N$, If the initial intermediate RO_2

Atmospheric
Chemistry
and Physics
Discussions
Open Access
EGU

639   is capable to proceed via autoxidation by the formal addition of O_2, we expect radicals,
640   $C_{10}H_{16}O_{5+2x}N$ (x denotes times of autoxidation performed) with an odd oxygen number,
641   to be formed (R5a). In addition, peroxy radicals with an even oxygen number,
642   $C_{10}H_{16}O_{6+2x}N$, are likely produced via reaction chain 5b: (1) RO_2 is propagated to RO
643   through bimolecular reactions, and (2) RO isomerize to an alcohol by internal H
644   abstraction forming a carbon-centered radical (Orlando et al., 2003;Orlando and
645   Tyndall, 2012), (3) the carbon-centered radical can again take up an oxygen molecule
646   and follow the autoxidation route. The $C_{10}H_{16}O_9N$ radical is also moderately intense in
647   the BVOCs-OOMs I factor (Fig. 9(a)), testifying the presence of NO_3 chemistry. These
648   $C_{10}H_{16}O_{6-11}N$ radicals are also reported in the CLOUD chamber (Yan et al., 2020). In
649   addition to C_{10} radicals, a C_5 radical, $C_5H_8O_5N$ (peak fitting are shown in Fig. S8), is
650   also found in the BVOCs-OOMs II factor. $C_5H_8O_5N$ are possibly derived from the
651   oxidation of isoprene initiated by NO_3, as observed in the laboratory (Zhao et al., 2020).
652   Another hypothesis is that $C_5H_8O_5N$ is formed from the fragmentation process of
653   monoterpenes.
654
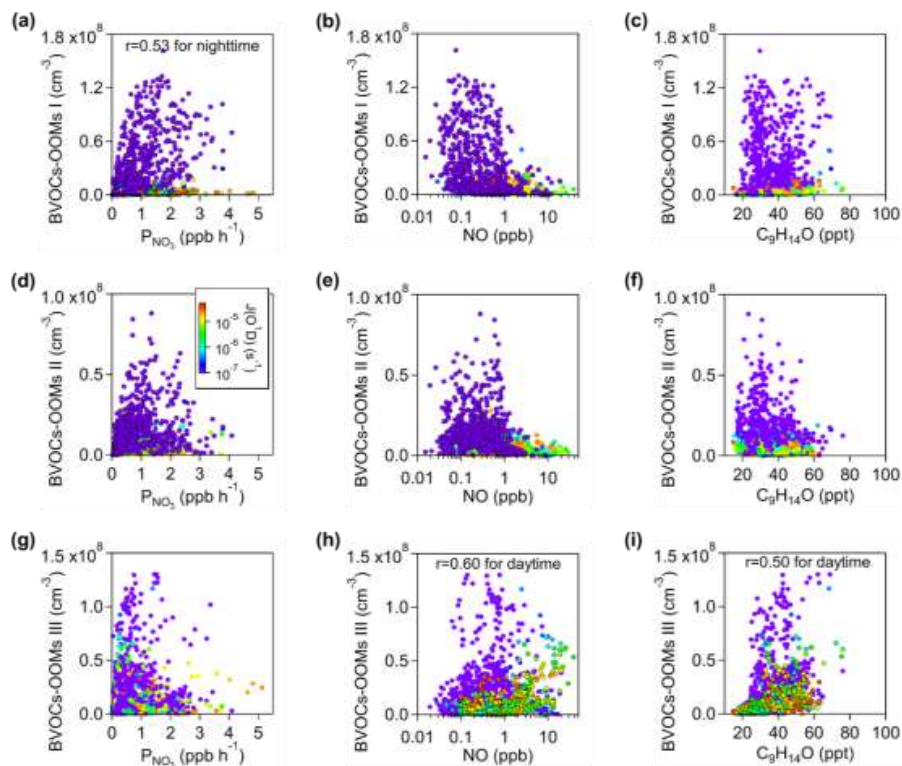
656   Figure 10. Scatter plots of the BVOCs-OOMs I factor with (a) P_{NO_3}, (b) NO, and (c)

657   nopinone ($C_9H_{14}O$). Scatter plots of the BVOCs-OOMs II factor with (d) P_{NO_3}, (e) NO,

658   and (f) nopinone ($C_9H_{14}O$). Scatter plots of the BVOCs-OOMs III factor with (g) P_{NO_3},

659   (h) NO, and (i) nopinone ($C_9H_{14}O$). All the scatters are colored by $J(O^1D)$, to show the

660   difference between day and night. Pearson correlation coefficient showed in (a) is

661   calculated for nighttime, but the correlation coefficients in (c) are only for daytime.

662

663   **BVOCs-OOMs III factor**

664

665   The third nighttime factor (BVOCs-OOMs III) is dominated by nitrogen-containing

666   species with a contribution ratio about 90%, among which dinitrates account for more

667   than 20% (Fig. 2(c)). When grouped by carbon numbers, C_{10} OOMs have the strongest

668   signal. Unlike the above two NO_3-related factors, this factor shows no correlation with

669   P_{NO3}, but has positive correlation with NO, especially during the daytime (Fig. 10(c)).

670     $C_9H_{14}O$, a typical product of NO-affected monoterpenes oxidation (Calogirou et al.,

671   1999), is found to be correlated with this factor (Fig. 10(c)). It is reasonable to infer that

672   these organic nitrates may come from terminations of monoterpenes-RO_2 by NO. In

673   addition to the elevated intensity during the nighttime, this factor still remains at a

674   relatively high concentration in the morning, which is much higher than that of the two

675   NO_3-related factors (Figure 9(e)). Owing to the suppression of NO to RO_2 autoxidation

676   and the relatively insufficient oxidant in dark environment, the effective OSc of the

677   BVOCs-OOMs III factor is lower than other factors. Apart from the mononitrates

678   summarized in Tabel S10, the $C_{10}H_{16}O_{7-10}N_2$ (dinitrates) and $C_{10}H_{17}O_{10}N_3$ (a trinitrate

679   charged by NO_3^- at m/z 401) are most likely the result of multiple-generation processes

680   involving OH or NO_3 oxidation of monoterpenes proceeding RO_2 + NO terminations.

681   A similar factor, called terpene nitrates, has also been reported in Centreville, USA

682   (Massoli et al., 2018), while in Hyytiälä, Finland (Yan et al., 2016), it's that the daytime

683   type-1 factor is related to NO.

684

685   **3.4 Nitrated phenols factors**

686

687   Nitrated phenols are of concern, because of their phytotoxicity (Rippen et al., 1987)

688   and as an important chromophores of brown carbon in aerosol (Desyaterik et al.,

689   2013;Mohr et al., 2013). The sources of these highly volatile compounds are attributed

690   to biomass burning, vehicle exhausts, and secondary gas or aqueous phase production

691   (Harrison et al., 2005). Here we identified three factors about NP, including the NP I

692   factor dominated by nitrophenol, the NP II factor dominated by substituted nitrophenols,

693   and the NP III factor dominated by dinitrophenols. Although the mass spectrum of the

694   NP III factor is less pure than the NP I & II factors (Fig. 11), its time series follows well

695   with $C_6H_4O_5N_2$ (Fig. 11(f)), implying that this factor is driven by di-nitrated-phenols

696   chemistry. Since nitrated phenols have been broadly investigated and relatively clearly

697   recognized (Harrison et al., 2005;Yuan et al., 2016;Wang et al., 2018b;Cheng et al.,

698   2021), they are not discussed too much here. It seems that the chemistry of nitrated

699   phenols is distinctive to other OOMs.

700
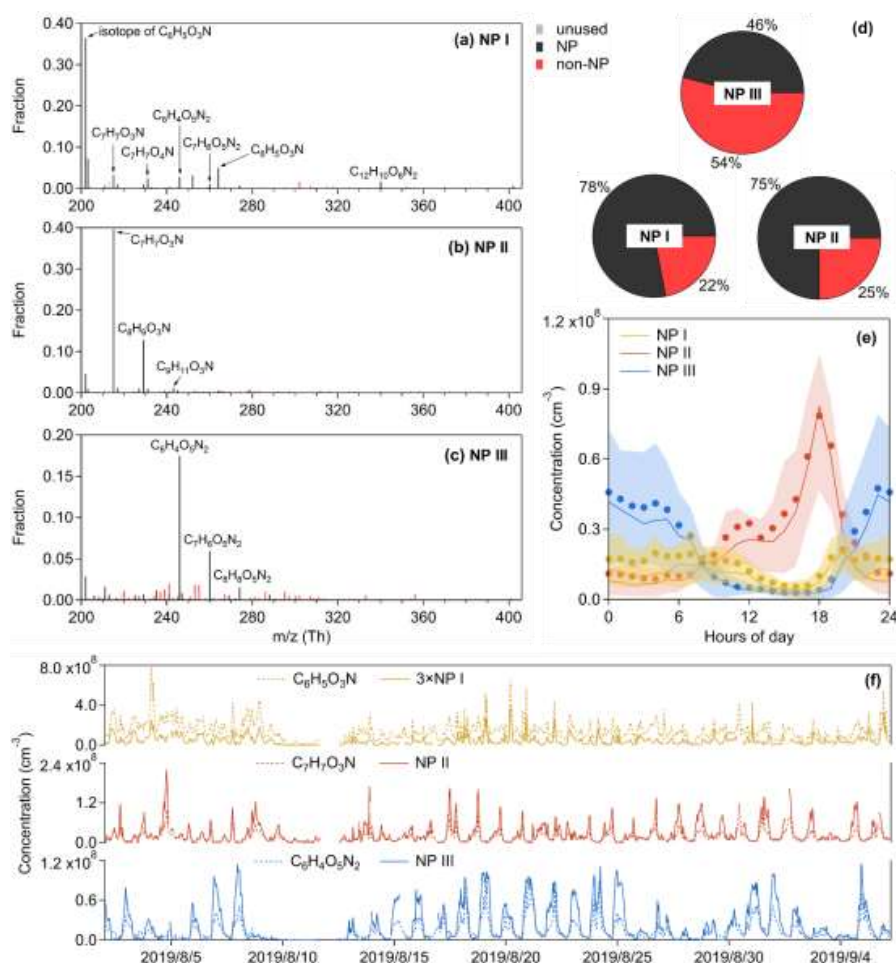
Figure 11. Mass spectra of (a) the NP I factor, (b) the NP II factor, and (c) the NP III factor, and the elemental formulas of major peaks are labeled above them. The gray sticks are fluorinated contaminations, or non-identified compounds. The nitrated phenols are drawn separately with black peaks in (a), (b) and (c), while other OOMs are plotted as red peaks. The molecules represented by the gray were not included in (d). Diurnal patterns of these three factors are shown in (e), the bold solid lines are the median values, shaded areas represent percentiles of 75 % and 25 % and solid circles represent mean values. (f) Time series of PMF factors and tracers.

3.5 Ensemble chemical properties

After performing PMF analysis, over 1000 non-nitro molecules have been identified through HR peaks fitting in each factor. The mean concentration of total non-nitro OOMs reconstructed from the selected PMF solution is about 2.1×10^8 molecules cm^{-3}. Ensemble chemical properties of these non-nitro OOMs are summarized in Fig. 12. The

717   number of carbon atoms implies the precursor information of OOMs. C_5 OOMs, which
718   principally consist of isoprene products benefited from the high reactivity and intensive
719   emissions of isoprene in summer, are the most abundant (Fig. 12(c)). While C_6-C_9
720   OOMs are mostly likely formed from the oxidation of AVOCs such as aromatics and
721   aliphatic series in the urban and suburban atmosphere, and as we expected, these
722   AVOCs-derived OOMs account for about 50% of the total signal (Fig. 12(c)). The
723   intensity of OOMs decreases from C_7 to C_9 determined by the concentration distribution
724   of precursors, but becomes a plateau at C_{10} (Fig. 12(c)), indicating another source of
725   C_{10} OOMs, such as monoterpenes oxidation. These results underscore the formation of
726   SOA precursors from a mixture of anthropogenic and biogenic emissions, under
727   ongoing forest cover increases (Wang et al., 2020a) in highly urbanized eastern China.
728
729   In addition to the anthropogenic VOCs, another human-induced perturbation on the
730   formation of OOMs is the NO_x-affected chemistry of VOCs, i.e., RO_2 + NO
731   terminations or NO_3-iniated oxidations. As showed in Fig. 12(c), about 70% of OOMs
732   are nitrogen-bearing compounds, regarded as organic nitrates within the allowed range
733   of uncertainty. If isoprene nitrates are not included, organic nitrates peak at C_7 as do the
734   nitrogen-free species, showing the significant production of organic nitrates through the
735   AVOCs + NO_x pathways. The NO_x effect on AVOCs-derived OOMs, typified by the
736   Aro-OOMs factor and the Aliph-OOMs factor, are not showed in previous ambient
737   measurements (Yan et al., 2016;Lee et al., 2016;Massoli et al., 2018).
738
739   OOMs grouped by carbon numbers or nitrogen numbers consistently have absolute
740   high concentrations in the daytime (Fig. 12(a) and (b)), revealing the crucial role of
741   photochemical progress, involving RO_2 + NO termination reactions, on OOMs. In
742   addition, The C_5-C_{10} OOMs are enhanced again during 19:00-22:00 LT, and the
743   nighttime peak of C_{10} OOMs is even higher than its daytime peak (Fig. 12(a)). The
744   nocturnal C_{10} OOMs are more intense than C_9 OOMs (Fig. 12(a)), and there are more
745   C_{10} nitrates than C_9 nitrates (Fig. 12(c)). These results show the fate of VOCs degraded
746   by NO_3 during the nighttime, which are more important to monoterpenes. In contrast to
747   nitrogen-free OOMs, organic nitrates are enriched through the reactions of BVOCs with
748   NO_3 in the early evening (Fig. 12(b)), as indicated by three BVOCs nighttime chemistry
749   factors.
750
751   Apart from reflecting the influence of NO_x, multi-nitrates also imply the multiple
752   generations of VOCs oxidation, which is evident in the products of isoprene (e.g.,
753   $C_5H_{10}O_8N_2$ and $C_5H_9O_{10}N_3$) due to its two carbon-carbon double bonds. As products of
754   mononitrates, multi-nitrates follow mononitrates in diurnal variation, with double peaks
755   initiated by OH and NO_3 respectively (Fig. 12(b)). Considering that the formation of
756   organic nitrate is only a small branch of RO_2 + NO termination, the contribution of
757   multi-step oxidation should be larger than that shown in Fig. 12(c).
758
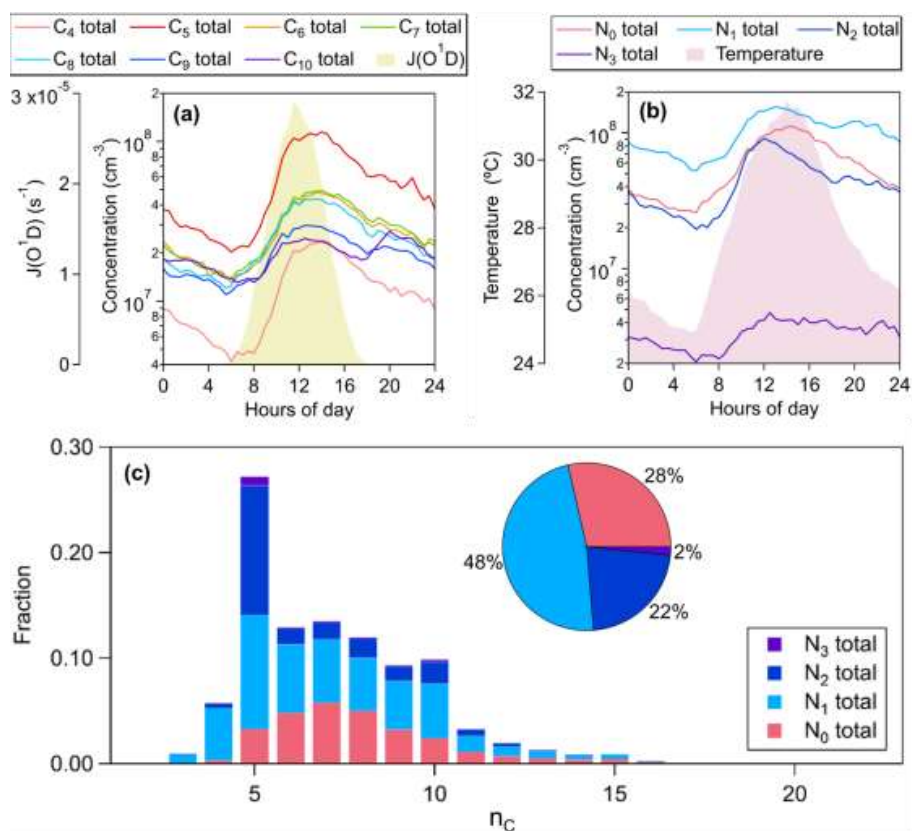
Figure 12. Ensemble chemical properties of non-nitro OOMs reconstructed from the selected PMF solution. (a) Median diurnal cycles of total compounds with carbon number of 5-10 respectively. (b) Median diurnal cycles of total compounds with n_N of 0-3 respectively. (c) The distributions of total observed OOMs at different n_C. OOMs on each carbon number is grouped by nitrogen number, and the total concentration fractions of each groups are reported in the pie chart. Since we selected peaks in the m/z range of 202-404 Th, OOMs with $n_C < 5$ or $n_C > 10$ detected by nitrate CI-APi-TOF are underestimated.

4 Conclusions

We have investigated the sources and characteristics of gas-phase OOMs observed using a nitrate CI-APi-TOF at the SORPES station in the YRD of eastern China, an environment dominated by anthropogenic emissions with enhanced biogenic emissions during summer.

The binPMF analysis, which avoids the uncertainty introduced by high-resolution peak fitting to the input data matrix, was applied to deconvolve the complexity of the data set, and it resolved 14 factors, among which 12 factors have been discussed in detail. A

779   morning factor (Aro-OOMs), correlated with the production rates of RO_2 from
780   aromatics, is characterized by unsaturated products of aromatics such as $C_xH_{2x-5}O_{6-9}N$
781   (x=6-12). An afternoon factor (Aliph-OOMs), containing the bulk of C_6-C_9 dinitrates
782   and trinitrates such as $C_xH_{2x-2}O_8N_2$ (x=4-13) and $C_xH_{2x}O_8N_2$ (x=4-8), is assumed to be
783   derived from aliphatics oxidation. A transported factor (Isop-OOMs), correlates with
784   MVK / MACR and SOA, is exclusively dominated by isoprene nitrates (e.g.,
785    $C_5H_{10}O_8N_2$ and $C_5H_9O_{10}N_3$). A nighttime factor (BVOCs-OOMs III), related to NO, is
786   dominated by terpenes nitrates such as $C_{10}H_{15}O_6N$, $C_{10}H_{16}O_{7-10}N_2$ and $C_{10}H_{17}O_{10}N_3$. In
787   addition to the factors distinguished by precursors, several factors are driven by
788   chemistry. A factor following the $J(O^1D)$ (Photo-related), consisting of isoprene
789   products mixed with others, is thought to be produced by in situ photochemistry. An
790   afternoon factor (Temp-related), having the most abundant nitrogen-free OOMs such
791   as $C_xH_{2x-4}O_{5-6}$ (x=5-10), $C_xH_{2x-2}O_5$ (x=5-10), and $C_xH_{2x-6}O_4$ (x=5-10), is generated
792   involving temperature-influenced chemistry. A daytime factor (O_x & SOA-related),
793   correlated well with O_x and SOA, indicates the photochemical aging process. Two
794   nighttime factors (BVOCs-OOMs I & II), benefiting from NO_3 and suppressed by NO,
795   are considered to be produced from NO_3-iniated oxidation of BVOCs, and both of them
796   have the fingerprint molecule, $C_{10}H_{16}O_9N$. The remaining three factors are governed
797   by nitrated phenols.

798

799   All of these factors from various precursors are influenced in different ways by NO_x.
800   Over 1000 non-nitro molecules have been identified and then reconstructed from
801   selected solution of binPMF, and about 72% of the total signal are contributed by
802   nitrogen-containing OOMs, almost regarded as organic nitrates formed through RO_2 +
803   NO terminations or NO_3-initiated oxidations. Moreover, multi-nitrates have a
804   contribution ratio of about 23% to total concentration, indicating the significant
805   presence of multiple oxidation generations, especially for isoprene (e.g., $C_5H_{10}O_8N_2$
806   and $C_5H_9O_{10}N_3$). The nitrate CI-APi-TOF data set presented here highlight the decisive
807   role of NO_x chemistry on OOMs formation in densely populated areas. In summary,
808   our findings highlight the dramatic interactions between anthropogenic and biogenic
809   emissions, and encourage more investigations from a mechanistic point of view.

810

811   The differences in OOMs observed in different environments are clear, and the
812   underlying causes are well worth considering. The precursors, oxidants, and formation
813   pathways of OOMs change when moving from urbanized areas to pristine regions, as
814   AVOCs and NOx concentrations decrease and BVOCs concentrations increase. This
815   process can also occur under the trend of global warming and anthropogenic emissions
816   mitigation, but we still know very little about it. Clarifying the variations of
817   composition, properties, and formation efficiency of OOMs will help to understand the
818   evolution of SOA production during this process.

819

Appendix A. The selected solution of binPMF analysis on nitrate CI-APi-TOF data
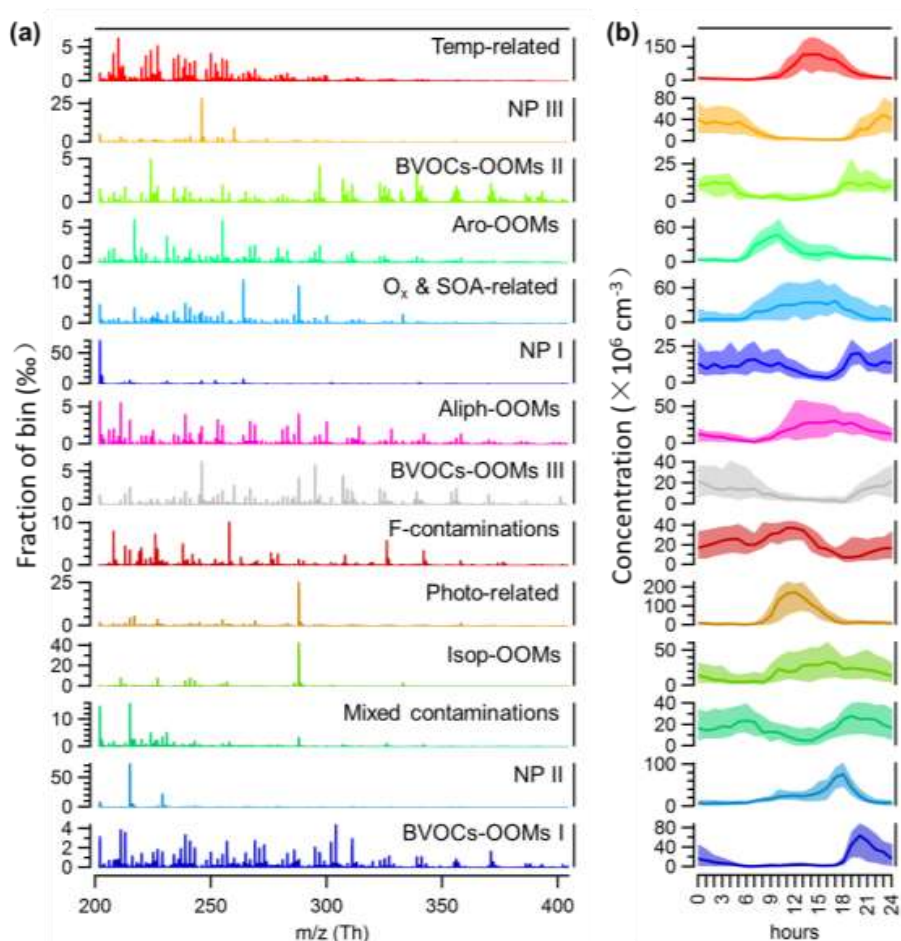
Figure A1. The selected solution for binPMF analysis of nitrate CI-APi-TOF data, showing (a) mass profile and (b) diurnal cycle of different factor.

826
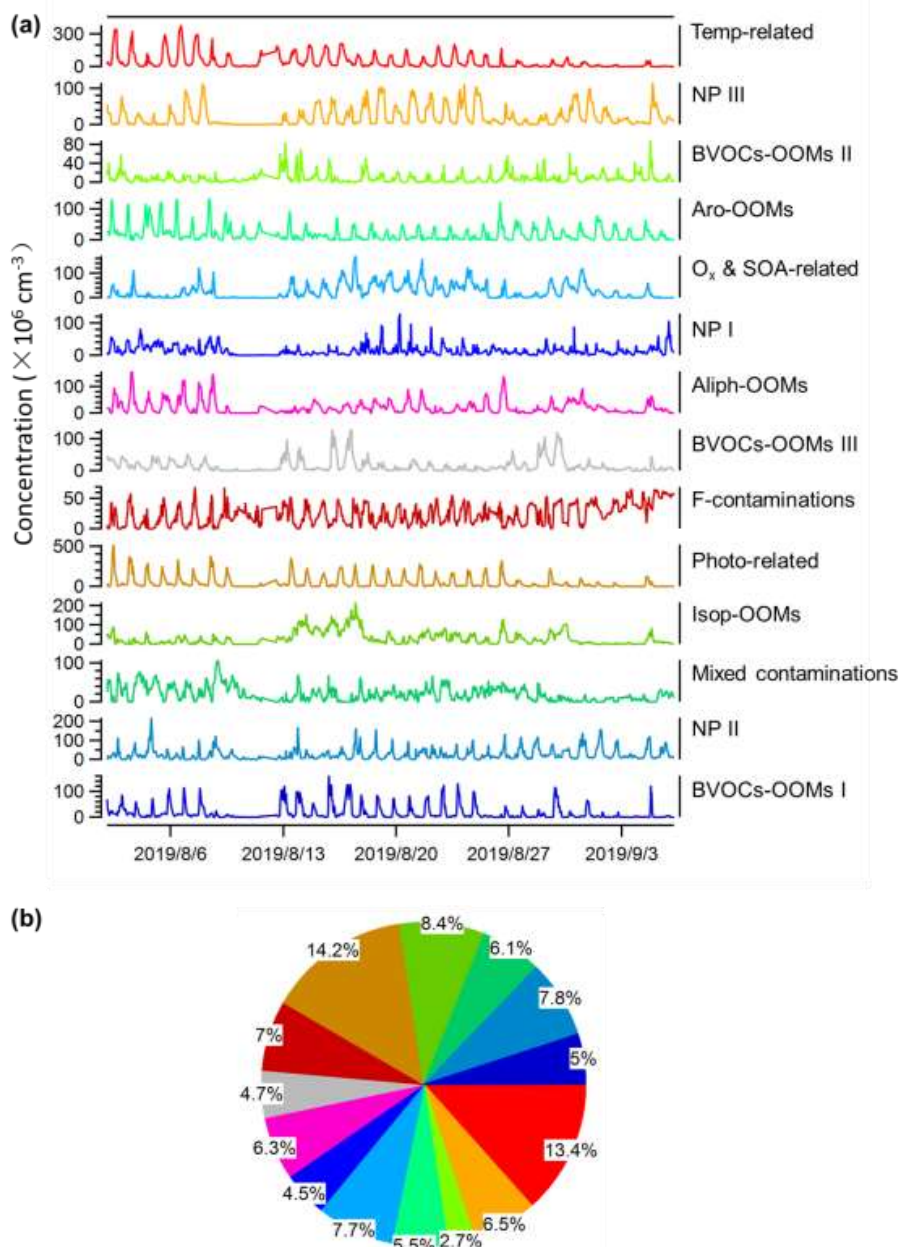
Figure A2. The selected solution for binPMF analysis of nitrate CI-APi-TOF, showing
(a) time series of and (b) contribution to total signal reconstructed by PMF of each
factor.

830

Data availability. Measurement data at the SORPES station, including OOMs data and
relevant trace gases and aerosol data as well as meteorological data, are available upon

833 request from the corresponding author before the SORPES database is open to the
834 public.
835
836 **Author contributions.**
837
838 **Competing interests.** The authors declare that they have no conflict of interest.
839

850
851 **Reference**
852

853 Atkinson, R.: Atmospheric chemistry of VOCs and NOx, Atmos. Environ., 34, 2063-
854 2101, 10.1016/s1352-2310(99)00460-4, 2000.
855 Ayres, B. R., Allen, H. M., Draper, D. C., Brown, S. S., Wild, R. J., Jimenez, J. L., Day,
856 D. A., Campuzano-Jost, P., Hu, W., de Gouw, J., Koss, A., Cohen, R. C., Duffey,
857 K. C., Romer, P., Baumann, K., Edgerton, E., Takahama, S., Thornton, J. A., Lee,
858 B. H., Lopez-Hilfiker, F. D., Mohr, C., Wennberg, P. O., Nguyen, T. B., Teng, A.,
859 Goldstein, A. H., Olson, K., and Fry, J. L.: Organic nitrate aerosol formation via
860 NO$_3$ + biogenic volatile organic compounds in the southeastern United States,
861 Atmos. Chem. Phys., 15, 13377-13392, 10.5194/acp-15-13377-2015, 2015.
862 Beck, L. J., Sarnela, N., Junninen, H., Hoppe, C. J. M., Garmash, O., Bianchi, F., Riva,
863 M., Rose, C., Peräkylä, O., Wimmer, D., Kausiala, O., Jokinen, T., Ahonen, L.,
864 Mikkilä, J., Hakala, J., He, X.-C., Kontkanen, J., Wolf, K. K. E., Cappelletti, D.,
865 Mazzola, M., Traversi, R., Petroselli, C., Viola, A. P., Vitale, V., Lange, R.,
866 Massling, A., Nøjgaard, J. K., Krejci, R., Karlsson, L., Zieger, P., Jang, S., Lee, K.,
867 Vakkari, V., Lampilahti, J., Thakur, R. C., Leino, K., Kangasluoma, J., Duplissy,
868 E.-M., Siivola, E., Marbouti, M., Tham, Y. J., Saiz-Lopez, A., Petäjä, T., Ehn, M.,
869 Worsnop, D. R., Skov, H., Kulmala, M., Kerminen, V.-M., and Sipilä, M.:
870 Differing mechanisms of new particle formation at two Arctic sites, Geophysical
871 Research Letters, 48, e2020GL091334, https://doi.org/10.1029/2020GL091334,
872 2021.
873 Berndt, T., Richters, S., Jokinen, T., Hyttinen, N., Kurten, T., Otkjaer, R. V., Kjaergaard,
874 H. G., Stratmann, F., Herrmann, H., Sipila, M., Kulmala, M., and Ehn, M.:
875 Hydroxyl radical-induced formation of highly oxidized organic compounds,
876 Nature Communications, 7, 10.1038/ncomms13677, 2016.

877   Bertram, T. H., Kimmel, J. R., Crisp, T. A., Ryder, O. S., Yatavelli, R. L. N., Thornton,
878   J. A., Cubison, M. J., Gonin, M., and Worsnop, D. R.: A field-deployable, chemical
879   ionization time-of-flight mass spectrometer, Atmos. Meas. Tech., 4, 1471-1479,
880   10.5194/amt-4-1471-2011, 2011.
881   Bianchi, F., Tröstl, J., Junninen, H., Frege, C., Henne, S., Hoyle, C. R., Molteni, U.,
882   Herrmann, E., Adamov, A., Bukowiecki, N., Chen, X., Duplissy, J., Gysel, M.,
883   Hutterli, M., Kangasluoma, J., Kontkanen, J., Kürten, A., Manninen, H. E., Münch,
884   S., Peräkylä, O., Petäjä, T., Rondo, L., Williamson, C., Weingartner, E., Curtius,
885   J., Worsnop, D. R., Kulmala, M., Dommen, J., and Baltensperger, U.: New particle
886   formation in the free troposphere: A question of chemistry and timing, Science,
887   352, 1109, 10.1126/science.aad5456, 2016.
888   Bianchi, F., Kurten, T., Riva, M., Mohr, C., Rissanen, M. P., Roldin, P., Berndt, T.,
889   Crounse, J. D., Wennberg, P. O., Mentel, T. F., Wildt, J., Junninen, H., Jokinen, T.,
890   Kulmala, M., Worsnop, D. R., Thornton, J. A., Donahue, N., Kjaergaard, H. G.,
891   and Ehn, M.: Highly oxygenated organic molecules (HOM) from gas-phase
892   autoxidation involving peroxy radicals: a key contributor to atmospheric aerosol,
893   Chem Rev, 10.1021/acs.chemrev.8b00395, 2019.
894   Birdsall, A. W., and Elrod, M. J.: Comprehensive NO-dependent study of the products
895   of the oxidation of atmospherically relevant aromatic compounds, The Journal of
896   Physical Chemistry A, 115, 5397-5407, 10.1021/jp2010327, 2011.
897   Bloss, C., Wagner, V., Jenkin, M. E., Volkamer, R., Bloss, W. J., Lee, J. D., Heard, D.
898   E., Wirtz, K., Martin-Reviejo, M., Rea, G., Wenger, J. C., and Pilling, M. J.:
899   Development of a detailed chemical mechanism (MCMv3.1) for the atmospheric
900   oxidation of aromatic hydrocarbons, Atmospheric Chemistry and Physics, 5, 641-
901   664, 10.5194/acp-5-641-2005, 2005.
902   Calogirou, A., Larsen, B. R., and Kotzias, D.: Gas-phase terpene oxidation products: a
903   review, Atmos. Environ., 33, 1423-1439, https://doi.org/10.1016/S1352-
904   2310(98)00277-5, 1999.
905   Canonaco, F., Crippa, M., Slowik, J. G., Baltensperger, U., and Prévôt, A. S. H.: SoFi,
906   an IGOR-based interface for the efficient use of the generalized multilinear engine
907   (ME-2) for the source apportionment: ME-2 application to aerosol mass
908   spectrometer data, Atmos. Meas. Tech., 6, 3649-3661, 10.5194/amt-6-3649-2013,
909   2013.
910   Cheng, X., Chen, Q., Li, Y., Huang, G., Liu, Y., Lu, S., Zheng, Y., Qiu, W., Lu, K., Qiu,
911   X., Bianchi, F., Yan, C., Yuan, B., Shao, M., Wang, Z., Canagaratna, M. R., Zhu,
912   T., Wu, Y., and Zeng, L.: Secondary production of gaseous nitrated phenols in
913   polluted urban environments, Environmental Science & Technology, 55, 4410-
914   4419, 10.1021/acs.est.0c07988, 2021.
915   Crounse, J. D., Nielsen, L. B., Jørgensen, S., Kjaergaard, H. G., and Wennberg, P. O.:
916   Autoxidation of organic compounds in the atmosphere, The Journal of Physical
917   Chemistry Letters, 4, 3513-3520, 10.1021/jz4019207, 2013.
918   Desyaterik, Y., Sun, Y., Shen, X., Lee, T., Wang, X., Wang, T., and Collett, J. L.:
919   Speciation of "brown" carbon in cloud water impacted by agricultural biomass

920   burning in eastern China, Journal of Geophysical Research: Atmospheres, 118,
921   7389-7399, 10.1002/jgrd.50561, 2013.

922   Ding, A., Nie, W., Huang, X., Chi, X., Sun, J., Kerminen, V.-M., Xu, Z., Guo, W., Petäjä,
923   T., Yang, X., Kulmala, M., and Fu, C.: Long-term observation of air pollution-
924   weather/climate interactions at the SORPES station: a review and outlook,
925   Frontiers of Environmental Science & Engineering, 10, 15, 10.1007/s11783-016-
926   0877-3, 2016.

927   Ding, A., Huang, X., Nie, W., Chi, X., Xu, Z., Zheng, L., Xu, Z., Xie, Y., Qi, X., Shen,
928   Y., Sun, P., Wang, J., Wang, L., Sun, J., Yang, X.-Q., Qin, W., Zhang, X., Cheng,
929   W., Liu, W., Pan, L., and Fu, C.: Significant reduction of PM2.5 in eastern China
930   due to regional-scale emission control: evidence from SORPES in 2011–2018,
931   Atmospheric Chemistry and Physics, 19, 11791-11801, 10.5194/acp-19-11791-
932   2019, 2019.

933   Ding, A. J., Fu, C. B., Yang, X. Q., Sun, J. N., Zheng, L. F., Xie, Y. N., Herrmann, E.,
934   Nie, W., Petäjä, T., Kerminen, V. M., and Kulmala, M.: Ozone and fine particle in
935   the western Yangtze River Delta: an overview of 1 yr data at the SORPES station,
936   Atmos. Chem. Phys., 13, 5813-5830, 10.5194/acp-13-5813-2013, 2013.

937   Ehn, M., Junninen, H., Petaja, T., Kurten, T., Kerminen, V. M., Schobesberger, S.,
938   Manninen, H. E., Ortega, I. K., Vehkamaki, H., Kulmala, M., and Worsnop, D. R.:
939   Composition and temporal behavior of ambient ions in the boreal forest,
940   Atmospheric Chemistry and Physics, 10, 8513-8530, 10.5194/acp-10-8513-2010,
941   2010.

942   Ehn, M., Kleist, E., Junninen, H., Petaja, T., Lonn, G., Schobesberger, S., Dal Maso,
943   M., Trimborn, A., Kulmala, M., Worsnop, D. R., Wahner, A., Wildt, J., and Mentel,
944   T. F.: Gas phase formation of extremely oxidized pinene reaction products in
945   chamber and ambient air, Atmospheric Chemistry and Physics, 12, 5113-5127,
946   10.5194/acp-12-5113-2012, 2012.

947   Ehn, M., Thornton, J. A., Kleist, E., Sipila, M., Junninen, H., Pullinen, I., Springer, M.,
948   Rubach, F., Tillmann, R., Lee, B., Lopez-Hilfiker, F., Andres, S., Acir, I. H.,
949   Rissanen, M., Jokinen, T., Schobesberger, S., Kangasluoma, J., Kontkanen, J.,
950   Nieminen, T., Kurten, T., Nielsen, L. B., Jorgensen, S., Kjaergaard, H. G.,
951   Canagaratna, M., Maso, M. D., Berndt, T., Petaja, T., Wahner, A., Kerminen, V.
952   M., Kulmala, M., Worsnop, D. R., Wildt, J., and Mentel, T. F.: A large source of
953   low-volatility secondary organic aerosol, Nature, 506, 476-479,
954   10.1038/nature13032, 2014.

955   Faxon, C., Hammes, J., Le Breton, M., Pathak, R. K., and Hallquist, M.:
956   Characterization of organic nitrate constituents of secondary organic aerosol (SOA)
957   from nitrate-radical-initiated oxidation of limonene using high-resolution
958   chemical ionization mass spectrometry, Atmos. Chem. Phys., 18, 5467-5481,
959   10.5194/acp-18-5467-2018, 2018.

960   Frege, C., Ortega, I. K., Rissanen, M. P., Praplan, A. P., Steiner, G., Heinritzi, M.,
961   Ahonen, L., Amorim, A., Bernhammer, A.-K., Bianchi, F., Brilke, S.,
962   Breitenlechner, M., Dada, L., Dias, A., Duplissy, J., Ehrhart, S., El-Haddad, I.,

963   Fischer, L., Fuchs, C., Garmash, O., Gonin, M., Hansel, A., Hoyle, C. R., Jokinen,
964   T., Junninen, H., Kirkby, J., Kürten, A., Lehtipalo, K., Leiminger, M., Mauldin, R.
965   L., Molteni, U., Nichman, L., Petäjä, T., Sarnela, N., Schobesberger, S., Simon,
966   M., Sipilä, M., Stolzenburg, D., Tomé, A., Vogel, A. L., Wagner, A. C., Wagner, R.,
967   Xiao, M., Yan, C., Ye, P., Curtius, J., Donahue, N. M., Flagan, R. C., Kulmala, M.,
968   Worsnop, D. R., Winkler, P. M., Dommen, J., and Baltensperger, U.: Influence of
969   temperature on the molecular composition of ions and charged clusters during pure
970   biogenic nucleation, Atmospheric Chemistry and Physics, 18, 65-79, 10.5194/acp-
971   18-65-2018, 2018.

972   Fu, X., Wang, S. X., Zhao, B., Xing, J., Cheng, Z., Liu, H., and Hao, J. M.: Emission
973   inventory of primary pollutants and chemical speciation in 2010 for the Yangtze
974   River Delta region, China, Atmos. Environ., 70, 39-50,
975   10.1016/j.atmosenv.2012.12.034, 2013.

976   Garmash, O., Rissanen, M. P., Pullinen, I., Schmitt, S., Kausiala, O., Tillmann, R., Zhao,
977   D., Percival, C., Bannan, T. J., Priestley, M., Hallquist, Å. M., Kleist, E., Kiendler-
978   Scharr, A., Hallquist, M., Berndt, T., McFiggans, G., Wildt, J., Mentel, T. F., and
979   Ehn, M.: Multi-generation OH oxidation as a source for highly oxygenated organic
980   molecules from aromatics, Atmospheric Chemistry and Physics, 20, 515-537,
981   10.5194/acp-20-515-2020, 2020.

982   Guo, Y., Yan, C., Li, C., Ma, W., Feng, Z., Zhou, Y., Lin, Z., Dada, L., Stolzenburg, D.,
983   Yin, R., Kontkanen, J., Daellenbach, K. R., Kangasluoma, J., Yao, L., Chu, B.,
984   Wang, Y., Cai, R., Bianchi, F., Liu, Y., and Kulmala, M.: Formation of nighttime
985   sulfuric acid from the ozonolysis of alkenes in Beijing, Atmos. Chem. Phys., 21,
986   5499-5511, 10.5194/acp-21-5499-2021, 2021.

987   Hallquist, M., Wenger, J. C., Baltensperger, U., Rudich, Y., Simpson, D., Claeys, M.,
988   Dommen, J., Donahue, N. M., George, C., Goldstein, A. H., Hamilton, J. F.,
989   Herrmann, H., Hoffmann, T., Iinuma, Y., Jang, M., Jenkin, M. E., Jimenez, J. L.,
990   Kiendler-Scharr, A., Maenhaut, W., McFiggans, G., Mentel, T. F., Monod, A.,
991   Prevot, A. S. H., Seinfeld, J. H., Surratt, J. D., Szmigielski, R., and Wildt, J.: The
992   formation, properties and impact of secondary organic aerosol: current and
993   emerging issues, Atmospheric Chemistry and Physics, 9, 5155-5236, 10.5194/acp-
994   9-5155-2009, 2009.

995   Harrison, M. A. J., Barra, S., Borghesi, D., Vione, D., Arsene, C., and Iulian Olariu, R.:
996   Nitrated phenols in the atmosphere: a review, Atmos. Environ., 39, 231-248,
997   https://doi.org/10.1016/j.atmosenv.2004.09.044, 2005.

998   Heinritzi, M., Simon, M., Steiner, G., Wagner, A. C., Kuerten, A., Hansel, A., and
999   Curtius, J.: Characterization of the mass-dependent transmission efficiency of a
1000   CIMS, Atmospheric Measurement Techniques, 9, 1449-1460, 10.5194/amt-9-
1001   1449-2016, 2016.

1002   Heinritzi, M., Dada, L., Simon, M., Stolzenburg, D., Wagner, A. C., Fischer, L., Ahonen,
1003   L. R., Amanatidis, S., Baalbaki, R., Baccarini, A., Bauer, P. S., Baumgartner, B.,
1004   Bianchi, F., Brilke, S., Chen, D., Chiu, R., Dias, A., Dommen, J., Duplissy, J.,
1005   Finkenzeller, H., Frege, C., Fuchs, C., Garmash, O., Gordon, H., Granzin, M., El

Haddad, I., He, X., Helm, J., Hofbauer, V., Hoyle, C. R., Kangasluoma, J., Keber, T., Kim, C., Kürten, A., Lamkaddam, H., Laurila, T. M., Lampilahti, J., Lee, C. P., Lehtipalo, K., Leiminger, M., Mai, H., Makhmutov, V., Manninen, H. E., Marten, R., Mathot, S., Mauldin, R. L., Mentler, B., Molteni, U., Müller, T., Nie, W., Nieminen, T., Onnela, A., Partoll, E., Passananti, M., Petäjä, T., Pfeifer, J., Pospisilova, V., Quéléver, L. L. J., Rissanen, M. P., Rose, C., Schobesberger, S., Scholz, W., Scholze, K., Sipilä, M., Steiner, G., Stozhkov, Y., Tauber, C., Tham, Y. J., Vazquez-Pufleau, M., Virtanen, A., Vogel, A. L., Volkamer, R., Wagner, R., Wang, M., Weitz, L., Wimmer, D., Xiao, M., Yan, C., Ye, P., Zha, Q., Zhou, X., Amorim, A., Baltensperger, U., Hansel, A., Kulmala, M., Tomé, A., Winkler, P. M., Worsnop, D. R., Donahue, N. M., Kirkby, J., and Curtius, J.: Molecular understanding of the suppression of new-particle formation by isoprene, Atmos. Chem. Phys., 20, 11809-11821, 10.5194/acp-20-11809-2020, 2020.

Herndon, S. C., Onasch, T. B., Wood, E. C., Kroll, J. H., Canagaratna, M. R., Jayne, J. T., Zavala, M. A., Knighton, W. B., Mazzoleni, C., Dubey, M. K., Ulbrich, I. M., Jimenez, J. L., Seila, R., de Gouw, J. A., de Foy, B., Fast, J., Molina, L. T., Kolb, C. E., and Worsnop, D. R.: Correlation of secondary organic aerosol with odd oxygen in Mexico City, Geophysical Research Letters, 35, 10.1029/2008gl034058, 2008.

Hu, W., Hu, M., Hu, W., Jimenez, J. L., Yuan, B., Chen, W., Wang, M., Wu, Y., Chen, C., Wang, Z., Peng, J., Zeng, L., and Shao, M.: Chemical composition, sources, and aging process of submicron aerosols in Beijing: Contrast between summer and winter, Journal of Geophysical Research: Atmospheres, 121, 1955-1977, 10.1002/2015jd024020, 2016.

Huang, R. J., Zhang, Y. L., Bozzetti, C., Ho, K. F., Cao, J. J., Han, Y. M., Daellenbach, K. R., Slowik, J. G., Platt, S. M., Canonaco, F., Zotter, P., Wolf, R., Pieber, S. M., Bruns, E. A., Crippa, M., Ciarelli, G., Piazzalunga, A., Schwikowski, M., Abbaszade, G., Schnelle-Kreis, J., Zimmermann, R., An, Z. S., Szidat, S., Baltensperger, U., El Haddad, I., and Prevot, A. S. H.: High secondary aerosol contribution to particulate pollution during haze events in China, Nature, 514, 218-222, 10.1038/nature13774, 2014.

Intergovernmental Panel on Climate, C.: Climate Change 2013 – The physical science basis: working group I contribution to the fifth assessment report of the Intergovernmental Panel on Climate Change, Cambridge University Press, Cambridge, 2014.

Jenkin, M. E., Young, J. C., and Rickard, A. R.: The MCM v3.3.1 degradation scheme for isoprene, Atmos. Chem. Phys., 15, 11433-11459, 10.5194/acp-15-11433-2015, 2015.

Jimenez, J. L., Canagaratna, M. R., Donahue, N. M., Prevot, A. S. H., Zhang, Q., Kroll, J. H., DeCarlo, P. F., Allan, J. D., Coe, H., Ng, N. L., Aiken, A. C., Docherty, K. S., Ulbrich, I. M., Grieshop, A. P., Robinson, A. L., Duplissy, J., Smith, J. D., Wilson, K. R., Lanz, V. A., Hueglin, C., Sun, Y. L., Tian, J., Laaksonen, A., Raatikainen, T., Rautiainen, J., Vaattovaara, P., Ehn, M., Kulmala, M., Tomlinson,

Atmospheric
Chemistry
and Physics
Discussions

J. M., Collins, D. R., Cubison, M. J., Dunlea, E. J., Huffman, J. A., Onasch, T. B., Alfarra, M. R., Williams, P. I., Bower, K., Kondo, Y., Schneider, J., Drewnick, F., Borrmann, S., Weimer, S., Demerjian, K., Salcedo, D., Cottrell, L., Griffin, R., Takami, A., Miyoshi, T., Hatakeyama, S., Shimono, A., Sun, J. Y., Zhang, Y. M., Dzepina, K., Kimmel, J. R., Sueper, D., Jayne, J. T., Herndon, S. C., Trimborn, A. M., Williams, L. R., Wood, E. C., Middlebrook, A. M., Kolb, C. E., Baltensperger, U., and Worsnop, D. R.: Evolution of organic aerosols in the atmosphere, Science, 326, 1525-1529, 10.1126/science.1180353, 2009.

Jokinen, T., Sipila, M., Junninen, H., Ehn, M., Lonn, G., Hakala, J., Petaja, T., Mauldin, R. L., III, Kulmala, M., and Worsnop, D. R.: Atmospheric sulphuric acid and neutral cluster measurements using CI-APi-TOF, Atmospheric Chemistry and Physics, 12, 4117-4125, 10.5194/acp-12-4117-2012, 2012.

Jokinen, T., Sipila, M., Richters, S., Kerminen, V. M., Paasonen, P., Stratmann, F., Worsnop, D., Kulmala, M., Ehn, M., Herrmann, H., and Berndt, T.: Rapid autoxidation forms highly oxidized RO_2 radicals in the atmosphere, Angew. Chem.-Int. Edit., 53, 14596-14600, 10.1002/anie.201408566, 2014.

Jokinen, T., Berndt, T., Makkonen, R., Kerminen, V. M., Junninen, H., Paasonen, P., Stratmann, F., Herrmann, H., Guenther, A. B., Worsnop, D. R., Kulmala, M., Ehn, M., and Sipila, M.: Production of extremely low volatile organic compounds from biogenic emissions: Measured yields and atmospheric implications, Proc Natl Acad Sci U S A, 112, 7123-7128, 10.1073/pnas.1423977112, 2015.

Junninen, H., Ehn, M., Petaja, T., Luosujarvi, L., Kotiaho, T., Kostiainen, R., Rohner, U., Gonin, M., Fuhrer, K., Kulmala, M., and Worsnop, D. R.: A high-resolution mass spectrometer to measure atmospheric ion composition, Atmospheric Measurement Techniques, 3, 1039-1053, 10.5194/amt-3-1039-2010, 2010.

Karl, T., Striednig, M., Graus, M., Hammerle, A., and Wohlfahrt, G.: Urban flux measurements reveal a large pool of oxygenated volatile organic compound emissions, Proceedings of the National Academy of Sciences, 115, 1186, 10.1073/pnas.1714715115, 2018.

Kirkby, J., Duplissy, J., Sengupta, K., Frege, C., Gordon, H., Williamson, C., Heinritzi, M., Simon, M., Yan, C., Almeida, J., Trostl, J., Nieminen, T., Ortega, I. K., Wagner, R., Adamov, A., Amorim, A., Bernhammer, A. K., Bianchi, F., Breitenlechner, M., Brilke, S., Chen, X. M., Craven, J., Dias, A., Ehrhart, S., Flagan, R. C., Franchin, A., Fuchs, C., Guida, R., Hakala, J., Hoyle, C. R., Jokinen, T., Junninen, H., Kangasluoma, J., Kim, J., Krapf, M., Kurten, A., Laaksonen, A., Lehtipalo, K., Makhmutov, V., Mathot, S., Molteni, U., Onnela, A., Perakyla, O., Piel, F., Petaja, T., Praplan, A. P., Pringle, K., Rap, A., Richards, N. A. D., Riipinen, I., Rissanen, M. P., Rondo, L., Sarnela, N., Schobesberger, S., Scott, C. E., Seinfeld, J. H., Sipila, M., Steiner, G., Stozhkov, Y., Stratmann, F., Tome, A., Virtanen, A., Vogel, A. L., Wagner, A. C., Wagner, P. E., Weingartner, E., Wimmer, D., Winkler, P. M., Ye, P. L., Zhang, X., Hansel, A., Dommen, J., Donahue, N. M., Worsnop, D. R., Baltensperger, U., Kulmala, M., Carslaw, K. S., and Curtius, J.: Ion-induced nucleation of pure biogenic particles, Nature, 533, 521-+, 10.1038/nature17953,

Atmospheric
Chemistry
and Physics
Discussions

1092   2016.

1093 Kuerten, A., Rondo, L., Ehrhart, S., and Curtius, J.: Calibration of a chemical ionization
1094   mass spectrometer for the measurement of gaseous sulfuric acid, J. Phys. Chem.
1095   A, 116, 6375-6386, 10.1021/jp212123n, 2012.

1096 Kulmala, M., Kontkanen, J., Junninen, H., Lehtipalo, K., Manninen, H. E., Nieminen,
1097   T., Petaja, T., Sipila, M., Schobesberger, S., Rantala, P., Franchin, A., Jokinen, T.,
1098   Jarvinen, E., Aijala, M., Kangasluoma, J., Hakala, J., Aalto, P. P., Paasonen, P.,
1099   Mikkila, J., Vanhanen, J., Aalto, J., Hakola, H., Makkonen, U., Ruuskanen, T.,
1100   Mauldin, R. L., III, Duplissy, J., Vehkamaki, H., Back, J., Kortelainen, A., Riipinen,
1101   I., Kurten, T., Johnston, M. V., Smith, J. N., Ehn, M., Mentel, T. F., Lehtinen, K.
1102   E. J., Laaksonen, A., Kerminen, V.-M., and Worsnop, D. R.: Direct observations
1103   of   atmospheric   aerosol   nucleation,   Science,   339,   943-946,
1104   10.1126/science.1227385, 2013.

1105 Kwan, A. J., Chan, A. W. H., Ng, N. L., Kjaergaard, H. G., Seinfeld, J. H., and
1106   Wennberg, P. O.: Peroxy radical chemistry and OH radical production during the
1107   NO3-initiated oxidation of isoprene, Atmos. Chem. Phys., 12, 7499-7515,
1108   10.5194/acp-12-7499-2012, 2012.

1109 Lambe, A., Massoli, P., Zhang, X., Canagaratna, M., Nowak, J., Daube, C., Yan, C.,
1110   Nie, W., Onasch, T., Jayne, J., Kolb, C., Davidovits, P., Worsnop, D., and Brune,
1111   W.: Controlled nitric oxide production via O(1D)+N2O reactions for use in
1112   oxidation flow reactor studies, Atmos. Meas. Tech., 10, 2283-2298, 10.5194/amt-
1113   10-2283-2017, 2017.

1114 Lee, B. H., Lopez-Hilfiker, F. D., Mohr, C., Kurtén, T., Worsnop, D. R., and Thornton,
1115   J. A.: An iodide-adduct high-resolution time-of-flight chemical-ionization mass
1116   spectrometer: application to atmospheric inorganic and organic compounds,
1117   Environmental Science & Technology, 48, 6309-6317, 10.1021/es500362a, 2014.

1118 Lee, B. H., Mohr, C., Lopez-Hilfiker, F. D., Lutz, A., Hallquist, M., Lee, L., Romer, P.,
1119   Cohen, R. C., Iyer, S., Kurtén, T., Hu, W., Day, D. A., Campuzano-Jost, P., Jimenez,
1120   J. L., Xu, L., Ng, N. L., Guo, H., Weber, R. J., Wild, R. J., Brown, S. S., Koss, A.,
1121   de Gouw, J., Olson, K., Goldstein, A. H., Seco, R., Kim, S., McAvey, K., Shepson,
1122   P. B., Starn, T., Baumann, K., Edgerton, E. S., Liu, J., Shilling, J. E., Miller, D. O.,
1123   Brune, W., Schobesberger, S., Ambro, E. L., and Thornton, J. A.: Highly
1124   functionalized organic nitrates in the southeast United States: Contribution to
1125   secondary organic aerosol and reactive nitrogen budgets, Proceedings of the
1126   National Academy of Sciences, 113, 1516, 10.1073/pnas.1508108113, 2016.

1127 Li, Y., Nie, W., Liu, Y., Huang, D., Xu, Z., Peng, X., George, C., Yan, C., Tham, Y. J.,
1128   Yu, C., Xia, M., Fu, X., Wang, X., Xue, L., Wang, Z., Xu, Z., Chi, X., Wang, T.,
1129   and Ding, A.: Photoinduced production of chlorine molecules from titanium
1130   dioxide surfaces containing chloride, Environmental Science & Technology
1131   Letters, 7, 70-75, 10.1021/acs.estlett.9b00704, 2020.

1132 Lim, S. S., Vos, T., Flaxman, A. D., Danaei, G., Shibuya, K., Adair-Rohani, H., Amann,
1133   M., Anderson, H. R., Andrews, K. G., Aryee, M., Atkinson, C., Bacchus, L. J.,
1134   Bahalim, A. N., Balakrishnan, K., Balmes, J., Barker-Collo, S., Baxter, A., Bell,

M. L., Blore, J. D., Blyth, F., Bonner, C., Borges, G., Bourne, R., Boussinesq, M., Brauer, M., Brooks, P., Bruce, N. G., Brunekreef, B., Bryan-Hancock, C., Bucello, C., Buchbinder, R., Bull, F., Burnett, R. T., Byers, T. E., Calabria, B., Carapetis, J., Carnahan, E., Chafe, Z., Charlson, F., Chen, H. L., Chen, J. S., Cheng, A. T. A., Child, J. C., Cohen, A., Colson, K. E., Cowie, B. C., Darby, S., Darling, S., Davis, A., Degenhardt, L., Dentener, F., Des Jarlais, D. C., Devries, K., Dherani, M., Ding, E. L., Dorsey, E. R., Driscoll, T., Edmond, K., Ali, S. E., Engell, R. E., Erwin, P. J., Fahimi, S., Falder, G., Farzadfar, F., Ferrari, A., Finucane, M. M., Flaxman, S., Fowkes, F. G. R., Freedman, G., Freeman, M. K., Gakidou, E., Ghosh, S., Giovannucci, E., Gmel, G., Graham, K., Grainger, R., Grant, B., Gunnell, D., Gutierrez, H. R., Hall, W., Hoek, H. W., Hogan, A., Hosgood, H. D., Hoy, D., Hu, H., Hubbell, B. J., Hutchings, S. J., Ibeanusi, S. E., Jacklyn, G. L., Jasrasaria, R., Jonas, J. B., Kan, H. D., Kanis, J. A., Kassebaum, N., Kawakami, N., Khang, Y. H., Khatibzadeh, S., Khoo, J. P., Kok, C., Laden, F., Lalloo, R., Lan, Q., Lathlean, T., Leasher, J. L., Leigh, J., Li, Y., Lin, J. K., Lipshultz, S. E., London, S., Lozano, R., Lu, Y., Mak, J., Malekzadeh, R., Mallinger, L., Marcenes, W., March, L., Marks, R., Martin, R., McGale, P., McGrath, J., Mehta, S., Mensah, G. A., Merriman, T. R., Micha, R., Michaud, C., Mishra, V., Hanafiah, K. M., Mokdad, A. A., Morawska, L., Mozaffarian, D., Murphy, T., Naghavi, M., Neal, B., Nelson, P. K., Nolla, J. M., Norman, R., Olives, C., Omer, S. B., Orchard, J., Osborne, R., Ostro, B., Page, A., Pandey, K. D., Parry, C. D. H., Passmore, E., Patra, J., Pearce, N., Pelizzari, P. M., Petzold, M., Phillips, M. R., Pope, D., Pope, C. A., Powles, J., Rao, M., Razavi, H., Rehfuess, E. A., Rehm, J. T., Ritz, B., Rivara, F. P., Roberts, T., Robinson, C., Rodriguez-Portales, J. A., Romieu, I., Room, R., Rosenfeld, L. C., Roy, A., Rushton, L., Salomon, J. A., Sampson, U., Sanchez-Riera, L., Sanman, E., Sapkota, A., Seedat, S., Shi, P. L., Shield, K., Shivakoti, R., Singh, G. M., Sleet, D. A., Smith, E., Smith, K. R., Stapelberg, N. J. C., Steenland, K., Stockl, H., Stovner, L. J., Straif, K., Straney, L., Thurston, G. D., Tran, J. H., Van Dingenen, R., van Donkelaar, A., Veerman, J. L., Vijayakumar, L., Weintraub, R., Weissman, M. M., White, R. A., Whiteford, H., Wiersma, S. T., Wilkinson, J. D., Williams, H. C., Williams, W., Wilson, N., Woolf, A. D., Yip, P., Zielinski, J. M., Lopez, A. D., Murray, C. J. L., and Ezzati, M.: A comparative risk assessment of burden of disease and injury attributable to 67 risk factors and risk factor clusters in 21 regions, 1990-2010: a systematic analysis for the Global Burden of Disease Study 2010, Lancet, 380, 2224-2260, 10.1016/s0140-6736(12)61766-8, 2012.

Liu, Y., Nie, W., Xu, Z., Wang, T., Wang, R., Li, Y., Wang, L., Chi, X., and Ding, A.: Semi-quantitative understanding of source contribution to nitrous acid (HONO) based on 1 year of continuous observation at the SORPES station in eastern China, Atmos. Chem. Phys., 19, 13289-13308, 10.5194/acp-19-13289-2019, 2019.

Lu, Y., Yan, C., Fu, Y., Chen, Y., Liu, Y., Yang, G., Wang, Y., Bianchi, F., Chu, B., Zhou, Y., Yin, R., Baalbaki, R., Garmash, O., Deng, C., Wang, W., Liu, Y., Petäjä, T., Kerminen, V.-M., Jiang, J., Kulmala, M., and Wang, L.: A proxy for atmospheric daytime gaseous sulfuric acid concentration in urban Beijing, Atmospheric Chemistry and Physics, 19, 1971-1983, 10.5194/acp-19-1971-2019, 2019.

1179   Massoli, P., Stark, H., Canagaratna, M. R., Krechmer, J. E., Xu, L., Ng, N. L., Mauldin,
1180   R. L., III, Yan, C., Kimmel, J., Misztal, P. K., Jimenez, J. L., Jayne, J. T., and
1181   Worsnop, D. R.: Ambient Measurements of Highly Oxidized Gas-Phase
1182   Molecules during the Southern Oxidant and Aerosol Study (SOAS) 2013, Acs
1183   Earth and Space Chemistry, 2, 653-672, 10.1021/acsearthspacechem.8b00028,
1184   2018.
1185   Mauldin Iii, R. L., Berndt, T., Sipilä, M., Paasonen, P., Petäjä, T., Kim, S., Kurtén, T.,
1186   Stratmann, F., Kerminen, V. M., and Kulmala, M.: A new atmospherically relevant
1187   oxidant of sulphur dioxide, Nature, 488, 193-196, 10.1038/nature11278, 2012.
1188   McFiggans, G., Mentel, T. F., Wildt, J., Pullinen, I., Kang, S., Kleist, E., Schmitt, S.,
1189   Springer, M., Tillmann, R., Wu, C., Zhao, D., Hallquist, M., Faxon, C., Le Breton,
1190   M., Hallquist, A. M., Simpson, D., Bergstrom, R., Jenkin, M. E., Ehn, M.,
1191   Thornton, J. A., Alfarra, M. R., Bannan, T. J., Percival, C. J., Priestley, M., Topping,
1192   D., and Kiendler-Scharr, A.: Secondary organic aerosol reduced by mixture of
1193   atmospheric vapours, Nature, 565, 587-593, 10.1038/s41586-018-0871-y, 2019.
1194   Mehra, A., Wang, Y., Krechmer, J. E., Lambe, A., Majluf, F., Morris, M. A., Priestley,
1195   M., Bannan, T. J., Bryant, D. J., Pereira, K. L., Hamilton, J. F., Rickard, A. R.,
1196   Newland, M. J., Stark, H., Croteau, P., Jayne, J. T., Worsnop, D. R., Canagaratna,
1197   M. R., Wang, L., and Coe, H.: Evaluation of the chemical composition of gas- and
1198   particle-phase products of aromatic oxidation, Atmospheric Chemistry and
1199   Physics, 20, 9783-9803, 10.5194/acp-20-9783-2020, 2020.
1200   Mohr, C., Lopez-Hilfiker, F. D., Zotter, P., Prevot, A. S., Xu, L., Ng, N. L., Herndon, S.
1201   C., Williams, L. R., Franklin, J. P., Zahniser, M. S., Worsnop, D. R., Knighton, W.
1202   B., Aiken, A. C., Gorkowski, K. J., Dubey, M. K., Allan, J. D., and Thornton, J. A.:
1203   Contribution of nitrated phenols to wood burning brown carbon light absorption
1204   in Detling, United Kingdom during winter time, Environ Sci Technol, 47, 6316-
1205   6324, 10.1021/es400683v, 2013.
1206   Molteni, U., Bianchi, F., Klein, F., El Haddad, I., Frege, C., Rossi, M. J., Dommen, J.,
1207   and Baltensperger, U.: Formation of highly oxygenated organic molecules from
1208   aromatic compounds, Atmospheric Chemistry and Physics, 18, 1909-1921,
1209   10.5194/acp-18-1909-2018, 2018.
1210   Nah, T., Sanchez, J., Boyd, C. M., and Ng, N. L.: Photochemical aging of α-pinene and
1211   β-pinene secondary organic aerosol formed from nitrate radical oxidation,
1212   Environmental Science & Technology, 50, 222-231, 10.1021/acs.est.5b04594,
1213   2016.
1214   Nel, A.: Air pollution-related illness: Effects of particles, Science, 308, 804-806,
1215   10.1126/science.1108752, 2005.
1216   Newland, M. J., Bryant, D. J., Dunmore, R. E., Bannan, T. J., Acton, W. J. F., Langford,
1217   B., Hopkins, J. R., Squires, F. A., Dixon, W., Drysdale, W. S., Ivatt, P. D., Evans,
1218   M. J., Edwards, P. M., Whalley, L. K., Heard, D. E., Slater, E. J., Woodward-
1219   Massey, R., Ye, C., Mehra, A., Worrall, S. D., Bacak, A., Coe, H., Percival, C. J.,
1220   Hewitt, C. N., Lee, J. D., Cui, T., Surratt, J. D., Wang, X., Lewis, A. C., Rickard,
1221   A. R., and Hamilton, J. F.: Low-NO atmospheric oxidation pathways in a polluted

1222   megacity, Atmos. Chem. Phys., 21, 1613-1625, 10.5194/acp-21-1613-2021, 2021.

1223   Ng, N. L., Kwan, A. J., Surratt, J. D., Chan, A. W. H., Chhabra, P. S., Sorooshian, A.,
1224   Pye, H. O. T., Crounse, J. D., Wennberg, P. O., Flagan, R. C., and Seinfeld, J. H.:
1225   Secondary organic aerosol (SOA) formation from reaction of isoprene with nitrate
1226   radicals (NO$_3$), Atmospheric Chemistry and Physics, 8, 4117-4140, 10.5194/acp-
1227   8-4117-2008, 2008.

1228   Nie, W., Ding, A. J., Xie, Y. N., Xu, Z., Mao, H., Kerminen, V. M., Zheng, L. F., Qi, X.
1229   M., Huang, X., Yang, X. Q., Sun, J. N., Herrmann, E., Petäjä, T., Kulmala, M., and
1230   Fu, C. B.: Influence of biomass burning plumes on HONO chemistry in eastern
1231   China, Atmospheric Chemistry and Physics, 15, 1147-1159, 10.5194/acp-15-
1232   1147-2015, 2015.

1233   Orlando, J. J., Tyndall, G. S., and Wallington, T. J.: The atmospheric chemistry of
1234   alkoxy radicals, Chemical Reviews, 103, 4657-4689, 10.1021/cr020527p, 2003.

1235   Orlando, J. J., and Tyndall, G. S.: Laboratory studies of organic peroxy radical
1236   chemistry: an overview with emphasis on recent issues of atmospheric
1237   significance, Chemical Society Reviews, 41, 6294-6317, 10.1039/c2cs35166h,
1238   2012.

1239   Paatero, P., and Tapper, U.: Positve matrix factorization - a nonnegative factor model
1240   with optimal utilization of error-estimates of data values, Environmetrics, 5, 111-
1241   126, 10.1002/env.3170050203, 1994.

1242   Pye, H. O. T., D'Ambro, E. L., Lee, B., Schobesberger, S., Takeuchi, M., Zhao, Y.,
1243   Lopez-Hilfiker, F., Liu, J. M., Shilling, J. E., Xing, J., Mathur, R., Middlebrook,
1244   A. M., Liao, J., Welti, A., Graus, M., Warneke, C., de Gouw, J. A., Holloway, J. S.,
1245   Ryerson, T. B., Pollack, I. B., and Thornton, J. A.: Anthropogenic enhancements
1246   to production of highly oxygenated molecules from autoxidation, Proc. Natl. Acad.
1247   Sci. U. S. A., 116, 6641-6646, 10.1073/pnas.1810774116, 2019.

1248   Qi, X. M., Ding, A. J., Nie, W., Petäjä, T., Kerminen, V. M., Herrmann, E., Xie, Y. N.,
1249   Zheng, L. F., Manninen, H., Aalto, P., Sun, J. N., Xu, Z. N., Chi, X. G., Huang, X.,
1250   Boy, M., Virkkula, A., Yang, X. Q., Fu, C. B., and Kulmala, M.: Aerosol size
1251   distribution and new particle formation in the western Yangtze River Delta of
1252   China: 2 years of measurements at the SORPES station, Atmospheric Chemistry
1253   and Physics, 15, 12445-12464, 10.5194/acp-15-12445-2015, 2015.

1254   Riccobono, F., Schobesberger, S., Scott, C. E., Dommen, J., Ortega, I. K., Rondo, L.,
1255   Almeida, J., Amorim, A., Bianchi, F., Breitenlechner, M., David, A., Downard, A.,
1256   Dunne, E. M., Duplissy, J., Ehrhart, S., Flagan, R. C., Franchin, A., Hansel, A.,
1257   Junninen, H., Kajos, M., Keskinen, H., Kupc, A., Kuerten, A., Kvashin, A. N.,
1258   Laaksonen, A., Lehtipalo, K., Makhmutov, V., Mathot, S., Nieminen, T., Onnela,
1259   A., Petaja, T., Praplan, A. P., Santos, F. D., Schallhart, S., Seinfeld, J. H., Sipila,
1260   M., Spracklen, D. V., Stozhkov, Y., Stratmann, F., Tome, A., Tsagkogeorgas, G.,
1261   Vaattovaara, P., Viisanen, Y., Vrtala, A., Wagner, P. E., Weingartner, E., Wex, H.,
1262   Wimmer, D., Carslaw, K. S., Curtius, J., Donahue, N. M., Kirkby, J., Kulmala, M.,
1263   Worsnop, D. R., and Baltensperger, U.: Oxidation products of biogenic emissions
1264   contribute to nucleation of atmospheric particles, Science, 344, 717-721,

1265   10.1126/science.1243527, 2014.

1266 Richters, S., Herrmann, H., and Berndt, T.: Highly oxidized RO_2 radicals and
1267   consecutive products from the ozonolysis of three sesquiterpenes, Environmental
1268   Science & Technology, 50, 2354-2362, 10.1021/acs.est.5b05321, 2016.

1269 Rippen, G., Zietz, E., Frank, R., Knacker, T., and Klöpffer, W.: Do airborne nitrophenols
1270   contribute to forest decline?, Environmental Technology Letters, 8, 475-482,
1271   10.1080/09593338709384508, 1987.

1272 Rollins, A. W., Browne, E. C., Min, K. E., Pusede, S. E., Wooldridge, P. J., Gentner, D.
1273   R., Goldstein, A. H., Liu, S., Day, D. A., Russell, L. M., and Cohen, R. C.:
1274   Evidence for NO_x control over nighttime SOA formation, Science, 337, 1210,
1275   10.1126/science.1221520, 2012.

1276 Shen, Y., Virkkula, A., Ding, A., Wang, J., Chi, X., Nie, W., Qi, X., Huang, X., Liu, Q.,
1277   Zheng, L., Xu, Z., Petäjä, T., Aalto, P. P., Fu, C., and Kulmala, M.: Aerosol optical
1278   properties at SORPES in Nanjing, east China, Atmospheric Chemistry and Physics,
1279   18, 5265-5292, 10.5194/acp-18-5265-2018, 2018.

1280 Sindelarova, K., Granier, C., Bouarar, I., Guenther, A., Tilmes, S., Stavrakou, T., Müller,
1281   J. F., Kuhn, U., Stefani, P., and Knorr, W.: Global data set of biogenic VOC
1282   emissions calculated by the MEGAN model over the last 30 years, Atmospheric
1283   Chemistry and Physics, 14, 9317-9341, 10.5194/acp-14-9317-2014, 2014.

1284 Sun, P., Nie, W., Chi, X., Xie, Y., Huang, X., Xu, Z., Qi, X., Xu, Z., Wang, L., Wang,
1285   T., Zhang, Q., and Ding, A.: Two years of online measurement of fine particulate
1286   nitrate in the western Yangtze River Delta: influences of thermodynamics and
1287 N_2O_5 hydrolysis, Atmospheric Chemistry and Physics, 18, 17177-17190,
1288   10.5194/acp-18-17177-2018, 2018.

1289 Sun, P., Nie, W., Wang, T., Chi, X., Huang, X., Xu, Z., Zhu, C., Wang, L., Qi, X., Zhang,
1290   Q., and Ding, A.: Impact of air transport and secondary formation on haze
1291   pollution in the Yangtze River Delta: In situ online observations in Shanghai and
1292   Nanjing,   Atmos.   Environ.,   225,   117350,
1293   https://doi.org/10.1016/j.atmosenv.2020.117350, 2020.

1294 Takeuchi, M., and Ng, N. L.: Chemical composition and hydrolysis of organic nitrate
1295   aerosol formed from hydroxyl and nitrate radical oxidation of α-pinene and β-
1296   pinene, Atmos. Chem. Phys., 19, 12749-12766, 10.5194/acp-19-12749-2019,
1297   2019.

1298 Tsiligiannis, E., Hammes, J., Salvador, C. M., Mentel, T. F., and Hallquist, M.: Effect
1299   of NO_x on 1,3,5-trimethylbenzene (TMB) oxidation product distribution and
1300   particle formation, Atmospheric Chemistry and Physics, 19, 15073-15086,
1301   10.5194/acp-19-15073-2019, 2019.

1302 Wang, J., Nie, W., Cheng, Y., Shen, Y., Chi, X., Wang, J., Huang, X., Xie, Y., Sun, P.,
1303   Xu, Z., Qi, X., Su, H., and Ding, A.: Light absorption of brown carbon in eastern
1304   China based on 3-year multi-wavelength aerosol optical property observations and
1305   an improved absorption Ångström exponent segregation method, Atmos. Chem.
1306   Phys., 18, 9061-9074, 10.5194/acp-18-9061-2018, 2018a.

1307 Wang, J., Feng, L., Palmer, P. I., Liu, Y., Fang, S., Bosch, H., O'Dell, C. W., Tang, X.,
1308   Yang, D., Liu, L., and Xia, C.: Large Chinese land carbon sink estimated from
1309   atmospheric carbon dioxide data, Nature, 586, 720-723, 10.1038/s41586-020-
1310   2849-9, 2020a.
1311 Wang, L., Wang, X., Gu, R., Wang, H., Yao, L., Wen, L., Zhu, F., Wang, W., Xue, L.,
1312   Yang, L., Lu, K., Chen, J., Wang, T., Zhang, Y., and Wang, W.: Observations of
1313   fine particulate nitrated phenols in four sites in northern China: concentrations,
1314   source apportionment, and secondary formation, Atmospheric Chemistry and
1315   Physics, 18, 4349-4359, 10.5194/acp-18-4349-2018, 2018b.
1316 Wang, M., Chen, D., Xiao, M., Ye, Q., Stolzenburg, D., Hofbauer, V., Ye, P., Vogel, A.
1317   L., Mauldin, R. L., Amorim, A., Baccarini, A., Baumgartner, B., Brilke, S., Dada,
1318   L., Dias, A., Duplissy, J., Finkenzeller, H., Garmash, O., He, X.-C., Hoyle, C. R.,
1319   Kim, C., Kvashnin, A., Lehtipalo, K., Fischer, L., Molteni, U., Petäjä, T.,
1320   Pospisilova, V., Quéléver, L. L. J., Rissanen, M., Simon, M., Tauber, C., Tomé, A.,
1321   Wagner, A. C., Weitz, L., Volkamer, R., Winkler, P. M., Kirkby, J., Worsnop, D. R.,
1322   Kulmala, M., Baltensperger, U., Dommen, J., El-Haddad, I., and Donahue, N. M.:
1323   Photo-oxidation of aromatic hydrocarbons produces low-volatility organic
1324   compounds, Environmental Science & Technology, 54, 7911-7921,
1325   10.1021/acs.est.0c02100, 2020b.
1326 Wang, S., Wu, R., Berndt, T., Ehn, M., and Wang, L.: Formation of highly oxidized
1327   radicals and multifunctional products from the atmospheric oxidation of
1328   alkylbenzenes, Environ Sci Technol, 51, 8442-8449, 10.1021/acs.est.7b02374,
1329   2017.
1330 Wang, Y., Mehra, A., Krechmer, J. E., Yang, G., Hu, X., Lu, Y., Lambe, A., Canagaratna,
1331   M., Chen, J., Worsnop, D., Coe, H., and Wang, L.: Oxygenated products formed
1332   from OH-initiated reactions of trimethylbenzene: autoxidation and accretion,
1333   Atmospheric Chemistry and Physics, 20, 9563-9579, 10.5194/acp-20-9563-2020,
1334   2020c.
1335 Wang, Z., Ehn, M., Rissanen, M. P., Garmash, O., Quéléver, L., Xing, L., Monge-
1336   Palacios, M., Rantala, P., Donahue, N. M., Berndt, T., and Sarathy, S. M.: Efficient
1337   alkane oxidation under combustion engine and atmospheric conditions,
1338   Communications Chemistry, 4, 18, 10.1038/s42004-020-00445-3, 2021.
1339 Wayne, R. P., Barnes, I., Biggs, P., Burrows, J. P., Canosamas, C. E., Hjorth, J., Lebras,
1340   G., Moortgat, G. K., Perner, D., Poulet, G., Restelli, G., and Sidebottom, H.: The
1341   nitrated radical - physics, chemistry, and the atmosphere, Atmospheric
1342   Environment Part a-General Topics, 25, 1-203, 10.1016/0960-1686(91)90192-a,
1343   1991.
1344 Wennberg, P. O., Bates, K. H., Crounse, J. D., Dodson, L. G., McVay, R. C., Mertens,
1345   L. A., Nguyen, T. B., Praske, E., Schwantes, R. H., Smarte, M. D., St Clair, J. M.,
1346   Teng, A. P., Zhang, X., and Seinfeld, J. H.: Gas-phase reactions of isoprene and its
1347   major oxidation products, Chem Rev, 118, 3337-3390,
1348   10.1021/acs.chemrev.7b00439, 2018.
1349 Wood, E. C., Canagaratna, M. R., Herndon, S. C., Onasch, T. B., Kolb, C. E., Worsnop,

1350   D. R., Kroll, J. H., Knighton, W. B., Seila, R., Zavala, M., Molina, L. T., DeCarlo,
1351   P. F., Jimenez, J. L., Weinheimer, A. J., Knapp, D. J., Jobson, B. T., Stutz, J., Kuster,
1352   W. C., and Williams, E. J.: Investigation of the correlation between odd oxygen
1353   and secondary organic aerosol in Mexico City and Houston, Atmospheric
1354   Chemistry and Physics, 10, 8947-8968, 10.5194/acp-10-8947-2010, 2010.

1355 Xia, M., Peng, X., Wang, W., Yu, C., Sun, P., Li, Y., Liu, Y., Xu, Z., Wang, Z., Xu, Z.,
1356   Nie, W., Ding, A., and Wang, T.: Significant production of $ClNO_2$ and possible
1357   source of Cl_2 from N_2O_5 uptake at a suburban site in eastern China, Atmos. Chem.
1358   Phys., 20, 6147-6158, 10.5194/acp-20-6147-2020, 2020.

1359 Xie, Y., Ding, A., Nie, W., Mao, H., Qi, X., Huang, X., Xu, Z., Kerminen, V.-M., Petäjä,
1360   T., Chi, X., Virkkula, A., Boy, M., Xue, L., Guo, J., Sun, J., Yang, X., Kulmala, M.,
1361   and Fu, C.: Enhanced sulfate formation by nitrogen dioxide: Implications from in
1362   situ observations at the SORPES station, Journal of Geophysical Research:
1363   Atmospheres, 120, 12679-12694, 10.1002/2015jd023607, 2015.

1364 Xiong, F., McAvey, K. M., Pratt, K. A., Groff, C. J., Hostetler, M. A., Lipton, M. A.,
1365   Starn, T. K., Seeley, J. V., Bertman, S. B., Teng, A. P., Crounse, J. D., Nguyen, T.
1366   B., Wennberg, P. O., Misztal, P. K., Goldstein, A. H., Guenther, A. B., Koss, A. R.,
1367   Olson, K. F., de Gouw, J. A., Baumann, K., Edgerton, E. S., Feiner, P. A., Zhang,
1368   L., Miller, D. O., Brune, W. H., and Shepson, P. B.: Observation of isoprene
1369   hydroxynitrates in the southeastern United States and implications for the fate of
1370 NO_x, Atmos. Chem. Phys., 15, 11257-11272, 10.5194/acp-15-11257-2015, 2015.

1371 Xu, Z., Huang, X., Nie, W., Chi, X., Xu, Z., Zheng, L., Sun, P., and Ding, A.: Influence
1372   of synoptic condition and holiday effects on VOCs and ozone production in the
1373   Yangtze River Delta region, China, Atmos. Environ., 168, 112-124,
1374   10.1016/j.atmosenv.2017.08.035, 2017.

1375 Xu, Z., Huang, X., Nie, W., Shen, Y., Zheng, L., Xie, Y., Wang, T., Ding, K., Liu, L.,
1376   Zhou, D., Qi, X., and Ding, A.: Impact of biomass burning and vertical mixing of
1377   residual-layer aged plumes on ozone in the Yangtze River Delta, China: a tethered-
1378   balloon measurement and modeling study of a multiday ozone opisode, Journal of
1379   Geophysical Research: Atmospheres, 123, 11,786-711,803,
1380   10.1029/2018jd028994, 2018.

1381 Xu, Z. N., Nie, W., Liu, Y. L., Sun, P., Huang, D. D., Yan, C., Krechmer, J., Ye, P. L.,
1382   Xu, Z., Qi, X. M., Zhu, C. J., Li, Y. Y., Wang, T. Y., Wang, L., Huang, X., Tang, R.
1383   Z., Guo, S., Xiu, G. L., Fu, Q. Y., Worsnop, D., Chi, X. G., and Ding, A. J.:
1384   Multifunctional products of isoprene oxidation in polluted atmosphere and their
1385   contribution to SOA, Geophysical Research Letters, 48, 10.1029/2020gl089276,
1386   2021.

1387 Yan, C., Nie, W., Äijälä, M., Rissanen, M. P., Canagaratna, M. R., Massoli, P., Junninen,
1388   H., Jokinen, T., Sarnela, N., Häme, S. A. K., Schobesberger, S., Canonaco, F., Yao,
1389   L., Prévôt, A. S. H., Petäjä, T., Kulmala, M., Sipilä, M., Worsnop, D. R., and Ehn,
1390   M.: Source characterization of highly oxidized multifunctional compounds in a
1391   boreal forest environment using positive matrix factorization, Atmospheric
1392   Chemistry and Physics, 16, 12715-12731, 10.5194/acp-16-12715-2016, 2016.

Yan, C., Nie, W., Vogel, A. L., Dada, L., Lehtipalo, K., Stolzenburg, D., Wagner, R., Rissanen, M. P., Xiao, M., Ahonen, L., Fischer, L., Rose, C., Bianchi, F., Gordon, H., Simon, M., Heinritzi, M., Garmash, O., Roldin, P., Dias, A., Ye, P., Hofbauer, V., Amorim, A., Bauer, P. S., Bergen, A., Bernhammer, A. K., Breitenlechner, M., Brilke, S., Buchholz, A., Mazon, S. B., Canagaratna, M. R., Chen, X., Ding, A., Dommen, J., Draper, D. C., Duplissy, J., Frege, C., Heyn, C., Guida, R., Hakala, J., Heikkinen, L., Hoyle, C. R., Jokinen, T., Kangasluoma, J., Kirkby, J., Kontkanen, J., Kürten, A., Lawler, M. J., Mai, H., Mathot, S., Mauldin, R. L., Molteni, U., Nichman, L., Nieminen, T., Nowak, J., Ojdanic, A., Onnela, A., Pajunoja, A., Petäjä, T., Piel, F., Quéléver, L. L. J., Sarnela, N., Schallhart, S., Sengupta, K., Sipilä, M., Tomé, A., Tröstl, J., Väisänen, O., Wagner, A. C., Ylisirniö, A., Zha, Q., Baltensperger, U., Carslaw, K. S., Curtius, J., Flagan, R. C., Hansel, A., Riipinen, I., Smith, J. N., Virtanen, A., Winkler, P. M., Donahue, N. M., Kerminen, V. M., Kulmala, M., Ehn, M., and Worsnop, D. R.: Size-dependent influence of NO_x on the growth rates of organic aerosol particles, Science Advances, 6, eaay4945, 10.1126/sciadv.aay4945, 2020.

Yang, L., Nie, W., Liu, Y., Xu, Z., Xiao, M., Qi, X., Li, Y., Wang, R., Zou, J., Paasonen, P., Yan, C., Xu, Z., Wang, J., Zhou, C., Yuan, J., Sun, J., Chi, X., Kerminen, V.-M., Kulmala, M., and Ding, A.: Towards building a physical proxy for gas-phase sulfuric acid concentration based on its budget analysis in polluted Yangtze River Delta, east China, Environmental Science & Technology, https://doi.org/10.1021/acs.est.1c00738, 2021.

Yuan, B., Liggio, J., Wentzell, J., Li, S.-M., Stark, H., Roberts, J. M., Gilman, J., Lerner, B., Warneke, C., Li, R., Leithead, A., Osthoff, H. D., Wild, R., Brown, S. S., and de Gouw, J. A.: Secondary formation of nitrated phenols: insights from observations during the Uintah Basin Winter Ozone Study (UBWOS) 2014, Atmospheric Chemistry and Physics, 16, 2139-2153, 10.5194/acp-16-2139-2016, 2016.

Zaytsev, A., Koss, A. R., Breitenlechner, M., Krechmer, J. E., Nihill, K. J., Lim, C. Y., Rowe, J. C., Cox, J. L., Moss, J., Roscioli, J. R., Canagaratna, M. R., Worsnop, D. R., Kroll, J. H., and Keutsch, F. N.: Mechanistic study of the formation of ring-retaining and ring-opening products from the oxidation of aromatic compounds under urban atmospheric conditions, Atmospheric Chemistry and Physics, 19, 15117-15129, 10.5194/acp-19-15117-2019, 2019.

Zhang, Q., Jimenez, J. L., Canagaratna, M. R., Allan, J. D., Coe, H., Ulbrich, I., Alfarra, M. R., Takami, A., Middlebrook, A. M., Sun, Y. L., Dzepina, K., Dunlea, E., Docherty, K., DeCarlo, P. F., Salcedo, D., Onasch, T., Jayne, J. T., Miyoshi, T., Shimono, A., Hatakeyama, S., Takegawa, N., Kondo, Y., Schneider, J., Drewnick, F., Borrmann, S., Weimer, S., Demerjian, K., Williams, P., Bower, K., Bahreini, R., Cottrell, L., Griffin, R. J., Rautiainen, J., Sun, J. Y., Zhang, Y. M., and Worsnop, D. R.: Ubiquity and dominance of oxygenated species in organic aerosols in anthropogenically-influenced Northern Hemisphere midlatitudes, Geophysical Research Letters, 34, 6, 10.1029/2007gl029979, 2007.

1436   Zhang, Y., Tang, L., Croteau, P. L., Favez, O., Sun, Y., Canagaratna, M. R., Wang, Z.,
1437   Couvidat, F., Albinet, A., Zhang, H., Sciare, J., Prévôt, A. S. H., Jayne, J. T., and
1438   Worsnop, D. R.: Field characterization of the PM$_{2.5}$ Aerosol Chemical Speciation
1439   Monitor: insights into the composition, sources, and processes of fine particles in
1440   eastern China, Atmos. Chem. Phys., 17, 14501-14517, 10.5194/acp-17-14501-
1441   2017, 2017.
1442   Zhang, Y., Peräkylä, O., Yan, C., Heikkinen, L., Äijälä, M., Daellenbach, K. R., Zha,
1443   Q., Riva, M., Garmash, O., Junninen, H., Paatero, P., Worsnop, D., and Ehn, M.:
1444   A novel approach for simple statistical analysis of high-resolution mass spectra,
1445   Atmos. Meas. Tech., 12, 3761-3776, 10.5194/amt-12-3761-2019, 2019.
1446   Zhang, Y., Peräkylä, O., Yan, C., Heikkinen, L., Äijälä, M., Daellenbach, K. R., Zha,
1447   Q., Riva, M., Garmash, O., Junninen, H., Paatero, P., Worsnop, D., and Ehn, M.:
1448   Insights into atmospheric oxidation processes by performing factor analyses on
1449   subranges of mass spectra, Atmos. Chem. Phys., 20, 5945-5961, 10.5194/acp-20-
1450   5945-2020, 2020.
1451   Zhao, D., Pullinen, I., Fuchs, H., Schrade, S., Wu, R., Acir, I. H., Tillmann, R., Rohrer,
1452   F., Wildt, J., Guo, Y., Kiendler-Scharr, A., Wahner, A., Kang, S., Vereecken, L.,
1453   and Mentel, T. F.: Highly oxygenated organic molecules (HOM) formation in the
1454   isoprene oxidation by NO$_3$ radical, Atmos. Chem. Phys. Discuss., 2020, 1-28,
1455   10.5194/acp-2020-1178, 2020.
1456   Ziemann, P. J., and Atkinson, R.: Kinetics, products, and mechanisms of secondary
1457   organic aerosol formation, Chemical Society Reviews, 41, 6582-6605,
1458   10.1039/c2cs35122f, 2012.
1459